DEPARTMENT OF THE INTERIOR

GEOLOGICAL SURVEY

Preliminary assessment of paleoseismicity at White Sands Missile Range, southern New Mexico: Evidence for recency of faulting, fault segmentation, and repeat intervals for major earthquakes in the region

By

Michael N. Machette

Open-File Report 87-444

Prepared in cooperation with the U.S. Army Corp of Engineers
Experimental Waterways Station, Vicksburg, Mississippi

U.S. Geological Survey
Denver, CO 80225

1987

CONTENTS

ILLUSTRATIONS

PRELIMINARY ASSESSMENT OF PALEOSEISMICITY AT WHITE SANDS MISSILE RANGE, SOUTHERN NEW MEXICO: EVIDENCE FOR RECENCY OF FAULTING, FAULT SEGMENTATION, AND REPEAT INTERVALS FOR MAJOR EARTHQUAKES IN THE REGION

By Michael N. Machette

INTRODUCTION

The U.S. Department of Defense is siting a critical defense facility within the confines of the White Sands Missile Range (WSMR) in southern New Mexico. As part of the siting and design work, information is needed on the recency of faulting, on the average time intervals between major earthquakes (recurrence intervals), and on evidence for segmentation of long faults near White Sands Missile Range.

Morphometric data were collected from scarps on major range-bounding faulting near White Sands Missile Range by M.N. Machette, R.G. McGimsey, and M.F. Winter of the U.S. Geological Survey during the summers of 1980 and 1981. Earlier in 1979, Machette and S.M. Colman had collected data at the Cox Ranch site on the Organ Mountains fault near White Sands, New Mexico, during a field trip with Lee Gile (retired Soil Conservation Service), Bill Seager (New Mexico State University at Las Cruces), and John Hawley (New Mexico Bureau of Mines at Socorro). This reconnaissance work is part of an ongoing study of neotectonics of the Rio Grande rift in New Mexico, southeastern Arizona, and western Texas. Several abstracts (Machette and Colman, 1983; Machette, 1987), three 1:250,000-scale maps (Machette and McGimsey, 1983; Machette and Personius, 1984; Machette and others, 1986), and one reconnaissance compilation (Nakata and others, 1983) have been published for the rift; final compilation of about one half of the area remains to be completed. The data presented herein represent the first attempt to define the regional history of Quaternary faulting near White Sands Missile Range.

GEOLOGIC SETTING OF WHITE SANDS MISSILE RANGE

The pre-Pliocene geology of the region is only briefly discussed here because this report mostly concerns evidence for Quaternary faulting. This discussion focuses on the late Cenozoic structural and stratigraphic setting of the southern Rio Grande rift, from Socorro, N. Mex., to El Paso, Tex. In addition, some relevant aspects of the bedrock geology adjacent to major faults near the WSMR are discussed in regards to possible structural controls on fault geometry and fault segments and to amounts of net displacement across the faults. Published reports on this area include discussions of the evolution of the Rio Grande rift (Chapin and Seager, 1975; Bachman and Mehnert, 1978; Chapin, 1979; Cook and others, 1979; Seager and Morgan, 1979; Seager and others, 1984), and guidebooks and maps compiled by Fitzsimmons (1955), Seager and others (1975), Hawley (1978), Woodward and others (1978), Riecker (1979), Nakata and others (1982), and Baldridge and others (1983). The following discussion presents a broad overview of the Rio Grande rift in central and southern New Mexico, the timing of the rift's inception, and its

subsequent development during the late Cenozoic. Evidence for Quaternary faulting near WSMR is presented in view of the region's structural and geologic setting.

Rifting began 26-28 Ma in southern New Mexico (Chapin and Seager, 1975), as regional extension reactivated Paleozoic and Mesozoic zones of weakness (mainly faults and folds) along the Southern Rocky Mountains. A series of broad, northwest-trending, fault-bounded basins had formed by 26 Ma; these basins were filled in the Miocene by mafic flows, rhyolitic ash-flow tuffs, and locally derived alluvium. Seager and others (1984) postulated that this initial episode of rifting was in a back-arc setting, and was followed by period of renewed rifting during the late Miocene and Pliocene (9-3 Ma).

Quaternary and Pliocene faults, dikes, and volcanic events throughout the Rio Grande rift generally are oriented north-south, whereas Miocene faults and volcanic features commonly have a northwest orientation (Zoback and Zoback, 1980; Zoback and others, 1981; Aldrich and Laughlin, 1982; Laughlin and others, 1983; Lipman, 1983). These data strongly imply as much as 30° of clockwise rotation of the axis of least-principal stress during the past 30 Ma (Machette and Colman, 1983) Epeirogenic uplift of the region and blocking out of the north-trending basins and uplifts of the modern Rio Grande rift occurred during the latest period of extension.

Chapin and others (1978) mapped a transverse shear zone that extends through the Socorro area and trends east-northeast. This feature, also known as the Morenci lineament, marks a zone of differential rotation and step faulting, across which normal faults have opposite directions of displacement (north side--down to the east, south side--down to the west). This same relation is shown in major structural blocks: north of the zone, mid-Tertiary and older rocks of the Socorro and Lemitar Mountains, which bound the west side of the Rio Grande rift north of Socorro, dip steeply to the west, whereas in the Chupadera Mountains (southwest of Socorro and the transverse shear zone) the same age rocks dip to the east. This zone also coincides with an apparent right-lateral shift of the axial graben of the Rio Grande rift, just as the half grabens of the northern Rio Grande rift change tilt direction where the Jemez lineament crosses the Rio Grande rift in northern New Mexico (Muehlberger, 1979; Machette and Personius, 1984).

The rift changes from a single, narrow graben in the Socorro area, to an area of grabens (basins) and horsts (ranges) that are approximately 2.5 times wider than to the north. South of Socorro, the Rio Grande rift is expressed as three well defined graben systems: a western arm (the Winston graben); the central rift which extends from Socorro into the San Marcial, Engle, and Palomas basins; and an eastern arm (Tularosa and Hueco Basins) that extends from the latitude of Truth or Consequences south into Mexico (Ramberg and others, 1978; Seager and Morgan, 1979). The Rio Grande flows down the central rift in the Socorro area, and south through the San Marcial, Engle, and Palomas Basins to southern New Mexico. Faults that bound the Winston graben show no evidence of Quaternary movement; the basin and adjacent ranges, which trend northwest, are probably artifacts of late Miocene and early Pliocene extension.

Gravity and heat-flow data suggest that the Rio Grande rift is underlain by an asthenospheric upwarp that has thinned the crust throughout the length of the rift; the change to a dispersed graben system may be related to widening of this mantle upwarp from the Socorro area southward (Ramberg and others, 1978; Seager and Morgan, 1979). The surface expression of the Rio Grande rift is probably influenced by the type of physiography surrounding it; in central and northern New Mexico the rift is a single half or full graben between the stable regions of the Colorado Plateau to the west and the Great Plains to the east. However, in southern New Mexico the broad rift has topography similar to that of the Basin and Range province of Arizona (Cook and others, 1979). Although some authors believe that the Rio Grande rift merges imperceptibly with the Basin and Range province in southern New Mexico (Kelley, 1955; Elston and Bornhorst, 1979), recent geophysical data seems to infer the continuation of the thermotectonic conditions characteristic of the northern Rio Grande rift (for example, high heat flow, Quaternary faulting and volcanism, presence of deep basins) into southern New Mexico, westernmost Texas, and northern Mexico (Ramberg and others, 1978; Cook and others, 1979; Seager and Morgan, 1979). Most of the Basin and Range structures of southeastern Arizona have little evidence of Quaternary movement or activity (Machette and others, 1986).

Most of the WSMR lies within the Tularosa and Hueco Basins, which are bordered by the east-tilted Sacramento Mountains to the east and the west-tilted San Andres, Organ, and Franklin Mountains to the west (fig. 1). Both basin margins are marked by high-angle normal faults, which show substantial Pliocene and Pleistocene displacement. The abundance of Quaternary faults and thickness of upper Cenozoic sediments found in this elongate basin indicate a long period of active extension and uplift, as suggested by Seager and Morgan (1979). The Jornada del Muerto Basin lies between the Tularosa and Palomas/ Engle Basins, just east of the central rift of the Rio Grande and west of WSMR. This basin is bound on the west by the east-tilted Caballo and Fra Cristobal Mountains, and on the east by the San Andres Mountains. Only sparse evidence of Quaternary faulting is found along this basin margin, so it more of a syncline (sag) rather than a true graben (Kelley and Silver, 1952). The central rift basins (Palomas, Engle, and San Marcial) are bound on the east by major faults along the western margin of the Caballo and Fra Cristobal Mountains. These ranges and those adjacent WSMR are composed predominately of Paleozoic and Precambrian rocks The central rift is marked by a series of normal faults that cut middle to late Pleistocene alluvial deposits within and along the east side of the Palomas, Engle, and San Marcial Basins.

The thick sequence of sedimentary rocks of the Santa Fe Group preserved within the southern Rio Grande rift provides a stratigraphic record of faulting during the Miocene to the Pleistocene. North of Las Cruces, the Miocene Hayner Ranch and Rincon Valley Formations (Hawley and others, 1969; Seager and others, 1971; Chapin and Seager, 1975) of the lower part of the Santa Fe Group record the depositional response to initial rifting. These and coevil units exposed near Socorro (primarily the Popotosa Formation; Machette, 1978) were deposited in a series of large closed basins (bolsons).

Renewed extension coupled with regional epeirogenic uplift and an increase in runoff in the early Pliocene (Chapin, 1979) allowed the Rio Grande to become a major integrated system that flowed southward through southern Colorado and New Mexico to northern Mexico. As the Rio Grande and its

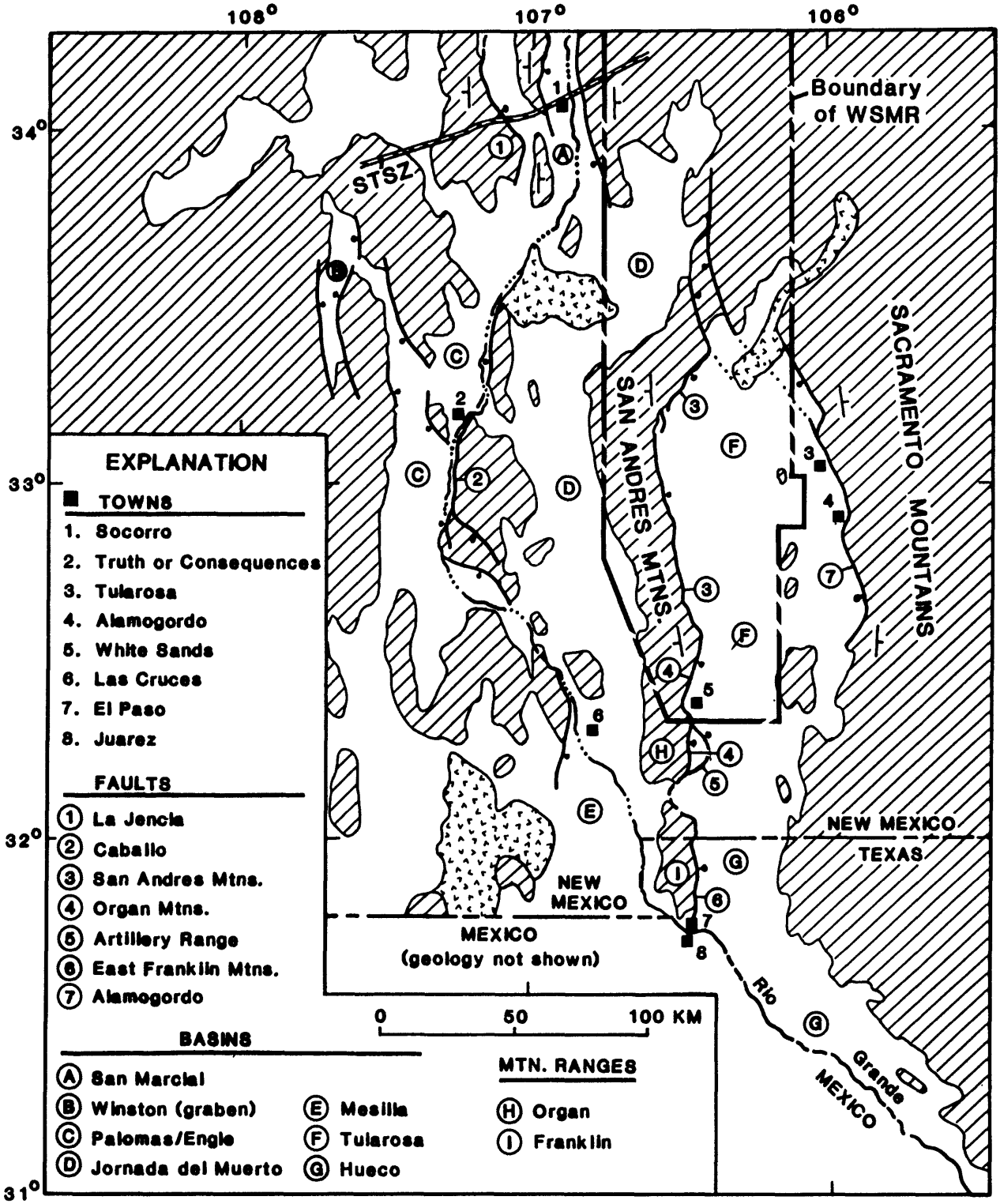

FIGURE 1.--Map showing geologic and geographic features near White Sands Missile Range (WSMR), southern New Mexico. Miocene and older rocks shown by cross-hatchure pattern, Quaternary volcanic rocks shown by V-pattern. Dip symbol indicates general direction of tilt of ranges bounding the rift. Only major range-bounding faults are shown. STSZ, Socorro transverse shear zone of Chapin and others (1978).

tributary streams traversed a series of elongate depressions (Hawley and Kottlowski, 1969; Hawley and others, 1969, 1976), they deposited a thick sequence of Pliocene and Pleistocene fluvial, bolson, and deltaic sediments (upper part of the Santa Fe Group), which are mapped as the Camp Rice Formation of Strain (1966) and Sierra Ladrones Formation (Machette, 1978). Deformation during or prior to the early Pliocene created an angular unconformity that locally separates the upper and lower parts of the Santa Fe Group.

Along the upper reach of the ancestral Rio Grande (those parts in New Mexico and Colorado), deposition in the rift basins continued from 4-5 Ma to about 0.7-0.5 Ma (Seager and others, 1984), when the upper and lower reaches of the Rio Grande were connected at El Paso, Tex. As a result of this integration, base level along the upper Rio Grande dropped drastically and, in response, the Rio Grande and its tributaries have cut deeply into basin-fill sediments and the underlying bedrock. The topography of the modern rift basins is strongly controlled by this downcutting. The top of the Sierra Ladrones and Camp Rice Formations are preserved as widespread relict basin floor and piedmont slope surfaces that are now 100-200 m above the Rio Grande and other major tributary streams (Bachman and Mehnert, 1978; Gile and others, 1981).

West of the Rio Grande, the medial and distal parts of huge, coalesced middle Pleistocene alluvial fan and piedmont aprons, the Cuchillo and Palomas Plains, spread eastward from the Black Range, Sierra Cuchillo, and the San Mateo Mountains (Lozinsky, 1986). East of the river, the Jornada del Muerto (spanish; journey of death) and Tularosa and Hueco Basins are largely undissected alluvial basin floors. Parts of these basins have been isolated from major aggradation or downcutting since the Rio Grande became entrenched in its present valley. The bulk of the surficial deposits in these two basins are of late Pleistocene and Holocene age.

METHODS FOR DETERMINING TIMES OF FAULTING

Two methods are used in this study to determine the times of fault movement. The first method is a stratigraphic approach by which the ages of the youngest faulted and oldest unfaulted deposits bracket the time of the most recent fault movement. Recurring episodes of movement are often recognized by comparing the cumulative amounts of displacement in deposits of different age. A second method is to infer ages of undated fault scarps through a quantitative comparison of their morphology with morphologies of dated scarps. This latter method is discussed in the section entitled "Fault-Scarp Morphology."

Stratigraphic Control

In preparing for reconnaissance work near WSMR, the surficial and young basin-fill deposits and faults in the map area were compiled from reports by Kelley (1955), Kottlowski (1955), Pray (1961), Weir (1965), Harbour (1972), Seager (1980, 1981), Wilson and Myers (1981), and from examination of aerial photographs. Since completing the fieldwork, Seager and others (1987) published a detailed map that shows the surficial and bedrock geology of the southern part of WSMR and their mapping has been incorporated into this study. For reconnaissance purposes, the Pliocene and younger deposits were

divided into four categories to provide age controls of fault movement. The oldest category, of Pliocene and early Pleistocene age (5.0-0.75 Ma) include some of the basaltic rocks of the region, and deposits of the Fort Hancock and Camp Rice formations. The middle Pleistocene (0.13-0.75 Ma) category includes those deposits forming the constructional surface of the Camp Rice Formation, which was abandoned about 0.5-0.7 Ma (Hawley and others, 1976; Seager and others, 1984)). These deposits also include units correlative with the Jornada I and Tortugas alluviums of Hawley and Kottlowski (1969) in southern New Mexico and the Kern Place alluvium of Kottlowski (1958) in the El Paso, Texas area. The upper Pleistocene (130,000-10,000 yr ago) category includes deposits correlative with the Isaack's Ranch, Picacho, and Jornada II alluviums (Hawley and Kottlowski, 1969); and the Gold Hill alluvium of Kottlowski (1958). The youngest category includes Holocene (<10,000 yr) alluvium of the lowest terraces and modern flood-plains (Fillmore alluvium of Hawley and Kottlowski, 1969) young alluvial-fan deposits (Organ alluvium of Hawley and Kottlowski, 1969), and eolian sand.

Because detailed maps showing surficial deposits are not available for the northern half of WSMR or the El Paso area, ages of the faulted deposits shown on the map were estimated from preservation of landforms, degree and density of dissection, stratigraphic and topographic position, and soil development (see Birkeland, 1984, for a discussion of dating criteria and methods). Although this investigation is mainly of a reconnaissance nature, I am confident that most of the age estimates for faulted and unfaulted deposits are reasonable because each category represents a broad range of geologic time (tens of thousands to hundreds of thousands of years).

Fault-Scarp Morphology

Stratigraphy and relative-dating techniques provide the chronologic framework for the Quaternary and Pliocene deposits that record faulting. However, the faulting may be considerably younger than the deposits that are affected (for example, a 5,000-yr-old scarp on 100,000-yr-old alluvium). However, analysis of fault-scarp degradation has given us a new tool that is appropriate for both reconnaissance and detailed investigations of faulting. Morphometric data from profiles of normal-fault scarps is used to determine the time elapsed since scarp formation. The empirical basis of this technique is simple: for two different-age scarps of comparable height and material (for example, a sandy gravel), the older scarp is the one having the more subdued topography, in terms of both slope and curvature. Calibration for determining the age of faulting comes from scarps and similar geomorphic features (shorelines and fluvial-terrace scarps) that are dated by radiometric or stratigraphic methods. This approach provides the time of the fault-scarp-forming event (earthquake) itself, rather than an age for a geomorphic surface or stratigraphic layer that may limit the time of last movement.

The approach used in this reconnaissance study is based on Bucknam and Anderson's (1979) empirical relation between the height of a fault scarp (H) and its maximum scarp-slope angle (θ), which followed the results of Wallace's (1977) studies of slope-degradation processes and the morphology of fault scarps. The scarp-morphology data presented in the following discussion show the relation between fault-scarp height and maximum scarp-slope angle, the variation of these two parameters, and their relation to fault scarps of known age. My studies are based on the following premises of fault-scarp evolution:

(1) initially, the free face of the fault scarp is nearly vertical, reflecting the near-surface dip of the fault; (2) the face soon slumps to the angle of repose of the faulted material, typically 32°-35° for unconsolidated surficial deposits; and (3) the slope of the scarp then decreases at a slower rate, mainly by the process of slopewash instead of gravational collapse (Wallace, 1977; Nash, 1981). Only those fault scarps on unconsolidated deposits, primarily of Quaternary age, have been analysed. Most of the fault scarps studied are on pebbly sand to sandy gravel alluvium, material that is generally of the same texture as scarps studied by Bucknam and Anderson (1979).

Scarp nomenclature and measurement of scarp profiles

The heights of fault scarps were determined from detailed topographic surveys made along traverses perpendicular to the scarps. I used a vernier-scale hand level and Jacobs staff, cloth tape, and stadia rod to measure slope angles across the scarp. These traverses extended 20-100 m above and below the fault scarp in order to determine the slopes of the adjacent alluvial surfaces. Measurements were made at intervals of 2-5 m on the upper and lower slopes and at intervals of 0.5-2 m on the scarp itself.

The nomenclature used in this report is modified only slightly from that used by Bucknam and Anderson (1979). Scarp height (H, in meters; fig. 2) is the vertical distance between the surfaces above and below the scarp where intersected by the plane representing the maximum scarp-slope angle (θ). The angles θ and γ denote the inclination from horizontal of the scarp and the adjacent land surfaces, respectively. The maximum scarp-slope angle was measured over a length equal to 10-20 percent of the distance between the crest and toe of the scarp at four to six locations within 3-5 m of each traverse line. The values of θ reported here are the averages of the repeated measurements; this averaging is necessary to minimize the influence of uncharacteristic determinations of θ. Thus, each traverse yielded a scarp profile and each profile yielded a value for H and θ (a data pair).

At least seven data pairs are needed for statistical analysis. Data sets smaller than seven may or may not represent the morphology of a fault scarp accurately; however, these smaller data sets are still useful to show local variation in height, steepness along the length of a fault scarp, and to characterize the general morphology of a fault scarp.

The height and maximum scarp-slope angle of an individual scarp was measured at several places along its length. Most heights range from about 1 to 10 m, but some older scarps are as much as 30 m high. I chose sites that are relatively stable (geomorphologically) by avoiding areas of active erosion or deposition. Much of the southern part of WSMR and south has an extensive cover of eolian sand that renders large tracts of ground unsuitable for studies of fault-scarp morphology. Discontinuous, en echelon, or segmented scarps (segments are sections of faults that each have a discrete history of surface rupture), were treated as individual scarps.

Major factors that affect the rate of scarp degradation include the texture and cohesion of the faulted deposits, orientation and height of the scarp, and the climate, vegetation, biologic activity, and topographic relief

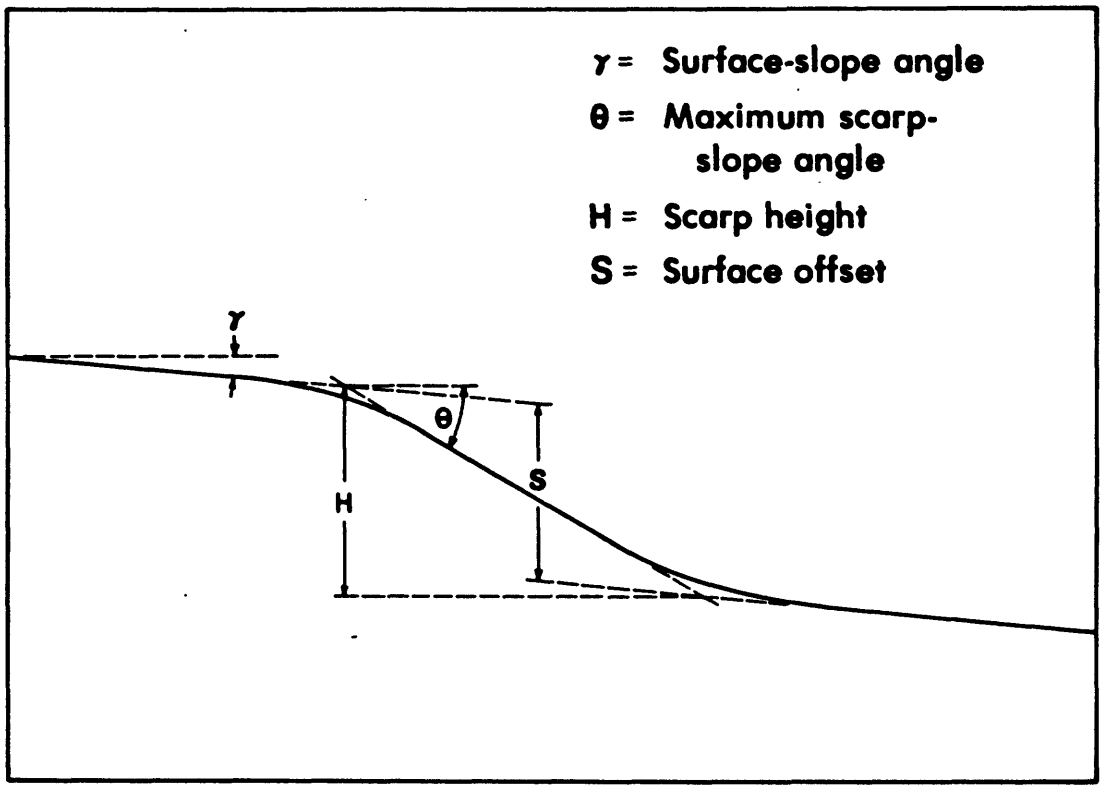

FIGURE 2.--Diagrammatic profile of a hypothetical fault-scarp (modified from Bucknam and Anderson, 1979, fig. 1).

at the scarp site (see Pierce and Colman, 1986, for a discussion of some of these factors). I chose profiling sites where these factors were as uniform as possible so that observed differences in scarp morphology would largely reflect the age of a scarp. Although variations exist between some scarps, especially in the texture of the faulted deposits, the measurements presented here represent typical fault scarps in the area.

Relation between maximum scarp-slope angle and scarp height

The studies of Bucknam and Anderson (1979) showed that there is a positive correlation between the heights of scarps (H) of a given age and their maximum scarp-slope angle (θ, fig. 3). The relation holds for a wide range of heights and slope angles (see recent discussion of Pierce and Colman, 1986) and also applies to fluvial scarps and wave-cut shorelines, such as those formed during the highest stand of Lake Bonneville in Utah. Although the Lake Bonneville shoreline escarpment is an erosional feature, Bucknam and Anderson (1979) consider that it eroded much like a fault scarp. The main difference in these two genetically different features is that a fault scarp requires a short time interval for the free face to collapse to the angle of repose, whereas a shoreline escarpment probably has an initial scarp-slope angle that is equal to, or slightly less than, the angle of repose (instead of nearly vertical). The time required for the scarp to degrade in such a manner has not been determined, but the degree of erosion of historic scarps in the Basin and Range province suggests to us that this interval is not more than a thousand years.

The empirical relation used here is based on a least-squares linear regression equation of the form $\theta=a+b(\log H)$ (where a is the value of θ when H=1 m and b is the slope of the line). Bucknam and Anderson (1979) found that 91 percent of the variation in the two parameters for 61 measurements of the Bonneville shoreline is explained by the equation, $\theta=3.8+21.0(\log H)$ (Bucknam, 1980). They also found that scarps younger and older than the Bonneville shoreline have similar relations, but plot in respectively higher and lower parts of the graph of θ versus H. The presentation of scarp-morphology data in this report follows the style of Bucknam and Anderson (1979) as illustrated in figure 3, which shows data from a hypothetical fault scarp. In this and other similarly constructed figures, data points are shown as circles or squares. Table 1 (see Appendix) shows the basic scarp-morphology data for major Quaternary faults near WSMR, and when there are an adequate number of data points, I also calculated the equation for the line of best fit and the coefficient of determination.

In reconnaissance studies of fault scarps in the Rio Grande rift there are three general conditions for which H and θ do not correlate very well. The first involves fault scarps having maximum scarp-slope angles (θ) that are only a few degrees steeper than the adjoining land surfaces; such scarps generally have a weak correlation between H and θ and a low value for the slope of the line of best fit (the value b). These scarps are either very small (<0.5 m) or are fairly old (for example, tens of thousands of years since last movement). The second condition involves scarps formed by faulting of surfaces having gradients (γ, fig. 3) of more than about 5°. Steeply sloping surfaces are usually associated with locally derived alluvial fan near the front of mountain ranges. This type of setting can cause the scarp to be

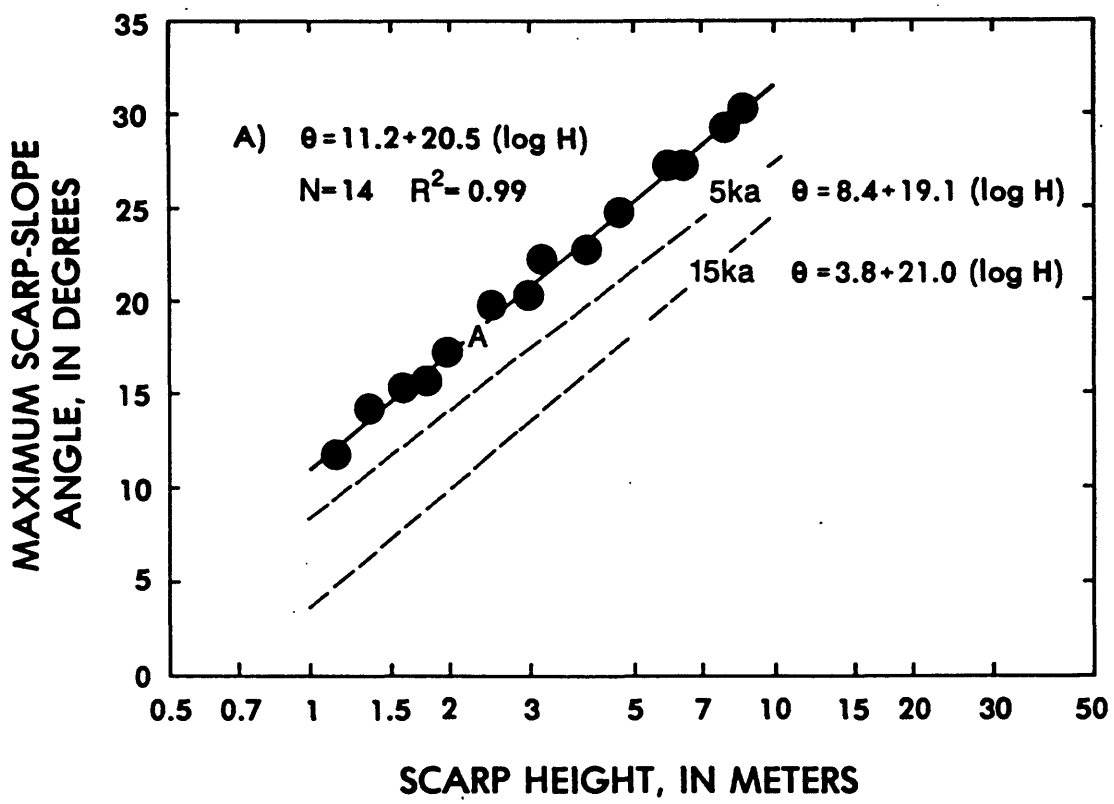

FIGURE 3.--Maximum scarp-slope angle (θ) plotted against scarp height (H) for a hypothetical fault scarp (from Machette and others, 1986). Also shown are the number of data pairs (n), the coefficient of determination (r^2), two reference lines for age comparisons (5 ka--La Jencia fault of central New Mexico; 15 ka--Bonneville shoreline of Utah), and equations for their lines of best fit.

anomalously steep and thus yield erroneously young age relations. The third condition involves young scarps having slope angles that exceed the angle of repose of the faulted material. In this case, the relation will apply only to small scarps that have slopes less than the angle of repose, whereas the large scarps will have slope angles that cluster about the angle of repose. Near WSMR, only the second condition (steep fan slopes) was encountered, and this problem is controlled by profiling only scarps on alluvial fans from deep canyons of the ranges.

The methods and results of Bucknam and Anderson (1979) and Machette and McGimsey (1983) were used to assign relative ages to fault scarps. For calibration we used the lines of best fit for data from two scarps of known age that are shown in figure 3. This figure (and a similar presentation in fig. 5) is the basis for comparison of scarp data throughout this report. The uppermost dashed line (labeled 5 ka in figs. 3 and 5) represents data from segment C of La Jencia fault near Magdalena, N. Mex. (most recent movement about 5 ka; Machette and McGimsey, 1983; Machette, 1986). This data set is represented by the equation, $\theta=11.2+20.5(\log H)$. The second dashed line (labeled 15 ka in figs. 3 and 5) is based on Bucknam's (1980) data from the highest wave-cut shoreline of Lake Bonneville, Utah, which is here considered to have formed about 15 ka on the basis of stratigraphic and radiometric studies by Scott and others (1983).

I use the following relatively conservative criteria to assign relative ages to fault scarps: scarps having (1) lines of best fit that lie above the upper dashed line on figure 3 (5 ka) are considered to be of Holocene age (less than 10 ka); (2) lines of best fit that lie between the two dashed lines indicate scarps of Holocene or latest Pleistocene age (less than 25 ka); and (3) lines of best fit that lie to the right of and below the lower dashed line (15 ka) indicate scarps of late Pleistocene age (10-130 ka) or, less likely, of middle Pleistocene age (130-750 ka).

Compound fault scarps

Most fault scarps in the map area, even those of less than 5-m height, were formed by more than one episode of faulting as shown by either increasing scarp heights in progressively older deposits or by scarps that have discrete facets--that is, compound-slope angles (fig. 4; Wallace, 1977). These compound scarps commonly have the form of degraded fault scarps that have been reactivated one or more times (the older scarp surfaces are denoted by the angle θ', fig. 4). Many of the compound scarps can be analyzed by assuming that the steepest element of the scarp (θ and Hs, fig. 4) was formed during the most recent episode of faulting and that the remaining less-steep parts marked by bevels represent previous periods of stability. In such cases, Hs is defined as the difference in elevation between the beveled scarp surfaces where intersected by the plane of the maximum slope. (Although this treatment violates the second of the three conditions previously stated--that slope gradients should be $<5°$--it is the most appropriate way to interpret compound slope angles.) A plot of Hs versus θ for a compound scarp and a plot of H versus θ for a single-event scarp along the same fault commonly will yield similar relations. When treated in such a manner, compound fault scarps yield values for Hs versus θ (open circles in fig. 5) that plot considerably younger than the data for Hm versus θ (filled circles in fig. 5) and are better

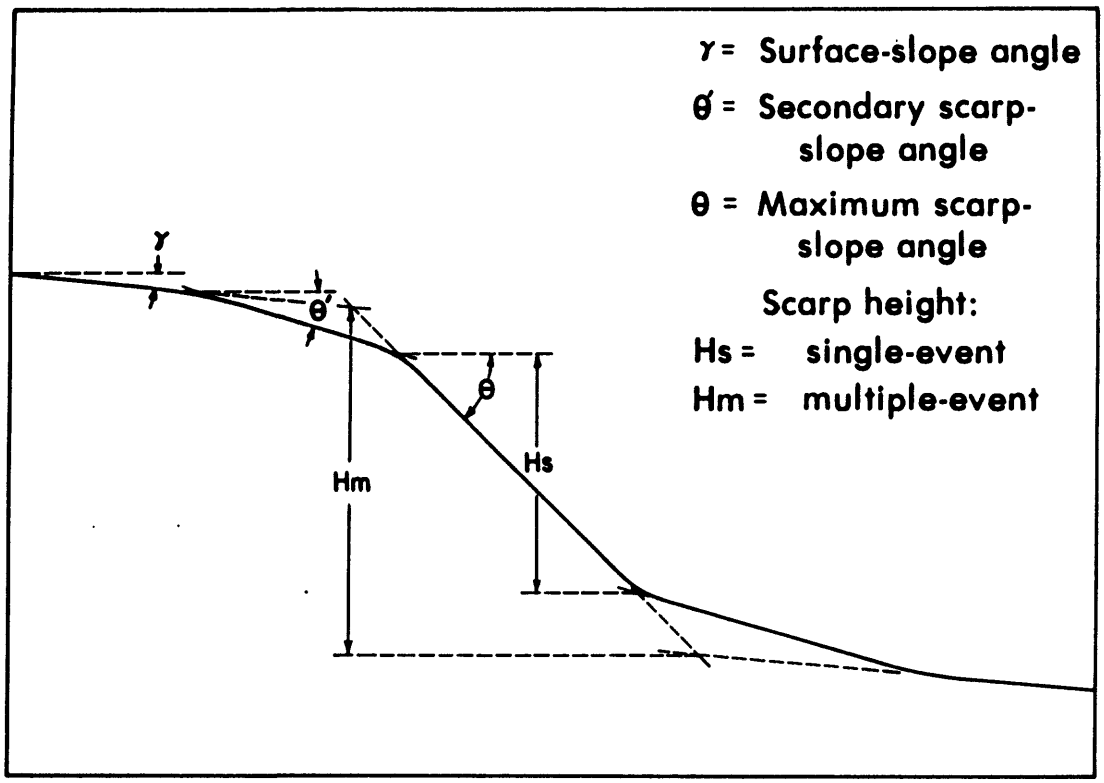

FIGURE 4.--Diagrammatic profile of a hypothetical compound fault scarp (from Machette and others, 1986).

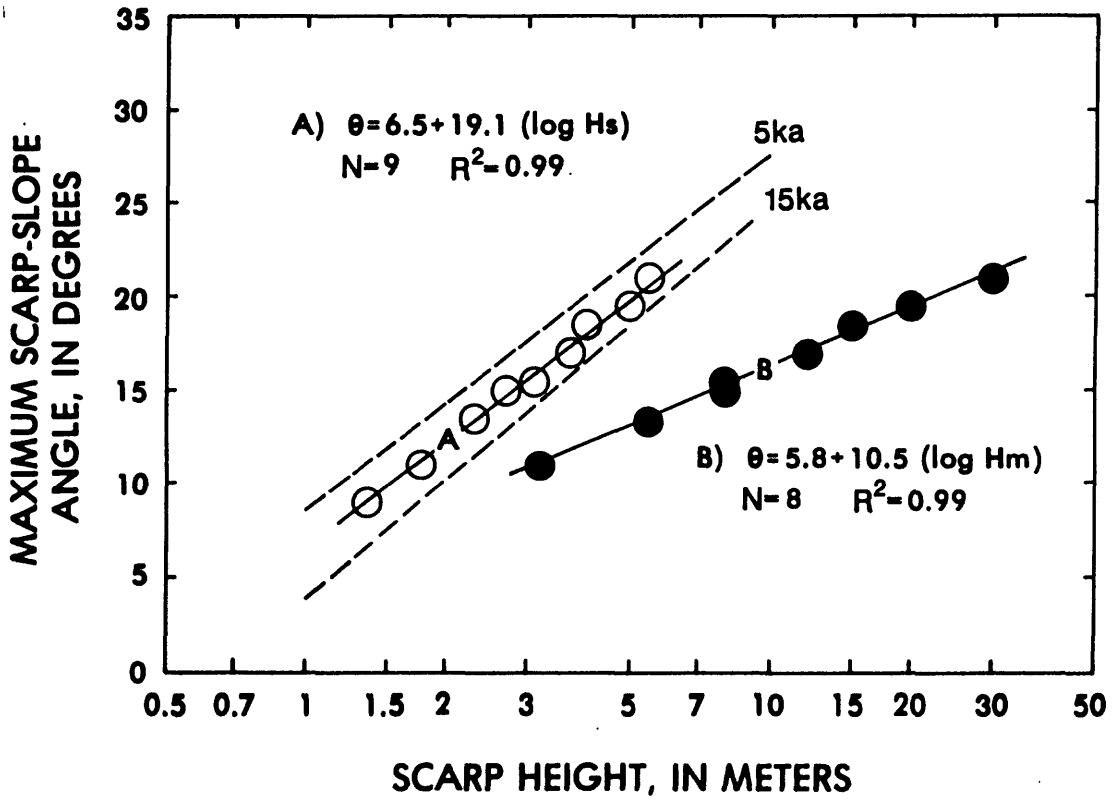

FIGURE 5.--Maximum scarp-slope angle (θ) plotted against scarp heights (Hs--open circles and line A; Hm--filled circles and line B) for a hypothetical compound fault scarp (from Machette and others, 1986). Also shown are the number of data pairs (n), the coefficient of determination (r^2), two reference lines for age comparisons (5 ka and 15 ka), and equations for their lines of best fit.

indicators of the recency of faulting than indicated by total scarp height (Ht). In such cases the sum of Hs and Hm will equal Ht.

The resultant lines of best fit for the youngest element of the scarps (Hs) commonly have steeper slopes (larger value for b in the regression equation) than do the data for the compound part of the fault scarp (Hm) or for the total scarp height (Ht; plotted as filled squares in some figures). In addition, the b values for plots of Hs versus θ for compound scarps are similar to those of H versus θ for single-event scarps. From these relations it seems reasonable to assume that fault-scarp data represented by a line of best fit having a low b value might indicate multiple episodes of faulting even though the scarp may not have obviously compound slope angles. Fault scarps as much as 20-60 m high clearly record ten's of individual faulting events. Compound angles (bevels) generally are preserved only when the most recent faulting event(s) is young compared to prior events (for example, 5 ka versus 25 ka). However, if the time of the most recent faulting (for example, 15 ka) approaches the time interval between faulting events (recurrence interval; 20 ka, prior event 35 ka) then the scarp formed by the most recent faulting will blend imperceptibly into the older scarp. Profiles across compound scarps may yield three measures of scarp height: Hs, single event; Hm, multiple event (compound part); and Ht, total scarp height where there is a compound part superposed on a large scarp (see table 1).

DISCUSSION OF PROMINENT FAULTS NEAR WHITE SANDS MISSILE RANGE

The San Andres-Organ-East Franklin Mountains fault system of Seager (1981) trends roughly north-south along the three major mountain ranges that border White Sands Missile Range on the west (fig. 1). When considered together, this system (or zone) of faults has a straight-line length of about 182 km: this length, and the it's history of repeated and relatively recent movement, make it the most impressive Quaternary fault zones in the interior of the United States. For comparison, the Wasatch fault zone of Utah and southern Idaho is 335 km long (length along trace is 370 km) and has 10-12 discrete fault segments that act independently of one another (Machette and others, 1986). In addition the Alamogordo fault, which lies at the western base of the Sacramento Mountains east of the WSMR, has repeated and young movement. Little modern or detailed work has been done on these faults, partly because most of their surface ruptures are within a restricted military zone. Our brief reconnaissance studies of these faults indicates that they have been recurrently active for at least the past 0.5 Ma. Although late Pleistocene or Holocene movement occurred on the faults, the most recent movement (middle to late? Holocene) is on the Organ Mountains fault.

The San Andres-Organ-East Franklin Mountains fault system separates upper Cenozoic basin-fill deposits (on the east) as much as 1.5 km in thickness (Seager and others, 1987) near the Organ Mountains from bedrock or thin basin-fill deposits that lie on bedrock on the uplifted block (west side) The throw on the fault system appears to increase from as much as 3 km along the San Andres Mountains (Kottlowski, 1955) and Franklin Mountains to 5 km or more along the Organ Mountains (Seager, 1981). Seager (1980, p 75-77) argued that the San Andres-Organ-East Franklin Mountains fault system on the west and the Alamogordo fault on the east (by analogy) are the product of basin-and-range-forming processes, and the basin-range structure is the combination of down

warping of the basin due to tensional forces, and the arching of Paleozoic strata to the east (the Sacramento Mountains) and west (the San Andres Mountains) This arching of Paleozoic strata also created antithetic Tertiary shear faults on the upthrown mountain blocks. The fault system has down-to-the-east displacement and dips 60°-70° E. where exposed. The west-dipping Almagordo fault, which lies at the western base of the Sacramento Mountains east of Alamogordo and Tularosa, N. Mex., partly defines the full-graben part of the Tularosa and Hueco Basins (fig. 1). South of Alamogordo, the Tularosa Basin becomes more of a half graben with bedrock extending well into the east half of the basin (Seager and others, 1987). Morphometric data for scarps along the Alamogordo fault suggest several faulting events in the late Pleistocene, and the most recent movement in the Holocene. Thus, both sides of the Tularosa Basin, and at least the west side of the Hueco Basin appear to be tectonically active parts of the Rio Grande rift. Most of the pertinent facts about these faults are summarized in table 2.

San Andres Mountains Fault

The San Andres Mountains fault (no. 3, fig. 1 and table 2) extends along the entire eastern flank of the San Andres Mountains and forms the western margin of the Tularosa Basin. Near New Mexico State Highway 70, the San Andres Mountains fault connects with the Organ Mountains fault which connects with the East Franklin Mountains fault south of WSMR (Seager, 1981; Seager and others, 1987). The San Andres Mountain fault trends north-northwest along most of its 106-km length. North of Rhodes Canyon, there is a 3-km gap in fault scarps; from there north, the fault strikes northeast to the vicinity of Sheep Mountain, where it again turns north and northwest (Kelley, 1955). Although military restrictions prevented Machette and Waters from examining the fault north of Rhodes Canyon, the embayed mountain front and extensive pediments developed along this section of the fault suggest that uplift has occurred at a much slower pace along the northernmost part the fault. In July 1987, I flew along the entire length of the fault, and found evidence of nearly continuous surface rupturing in late Pleistocene and older alluvium north to Salinas Peak and discontinuous ruptures as far north as Capital Peak (see detailed topographic maps of the area). The lack of fault scarps on the young (Holocene and perhaps latest Pleistocene) alluvial fans suggests that the section of the fault north of Rhodes Canyon was most recently active in the late Pleistocene (but not latest Pleistocene). Considering the gap in surface ruptures, change in orientation, and apparent lack of recent movement, the northern part San Andres Mountains fault probably represents a discrete segment of the fault, rather than a continuation of the fault that is prominent south of Rhodes Canyon.

If the scarps north of Rhodes Canyon represent the northern segment (22 km) of the San Andres Mountains fault, then the remaining 84 km of fault to the south probably contains more than one segment. From Rhodes Canyon southward, the east-facing fault scarps become morphologically less degraded (fresher) and those greater than 5-7 m in height show clear evidence of multiple movement (fig. 6; table 1). However, the scarps north of Lead Camp Canyon (profiles m18-12 and m18-14 to-20; figs. 7 and 8) appear more degraded than those even farther south. On the basis of scarp morphology (which is discussed in the following paragraphs), continuity of the scarps, and overall geometric pattern, I place a tentative segment boundary just west of the north end of Lake Lucero (near 106° W. and 32° N., Las Cruces 1° x 2° quadrangle).

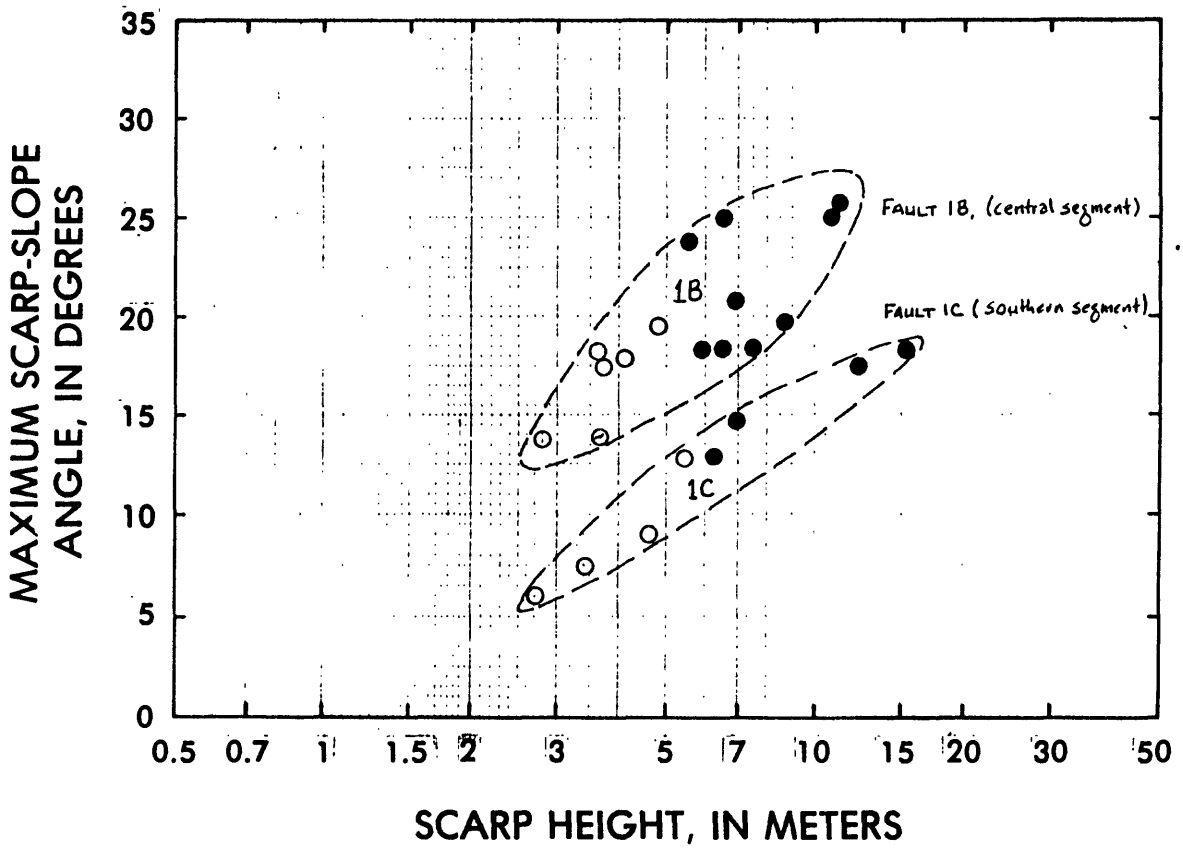

FIGURE 6.--Maximum scarp-slope angle (θ) plotted against scarp heights (Hs, open circles; Hm and Ht, filled circles) for the San Andres Mountain fault between Rhodes Canyon (on the north) and I-70 (on the south). Division of this part of the fault into two segments results in two discrete fields of scarp data (see figures 6 and 7). See table 1 for morphometric data.

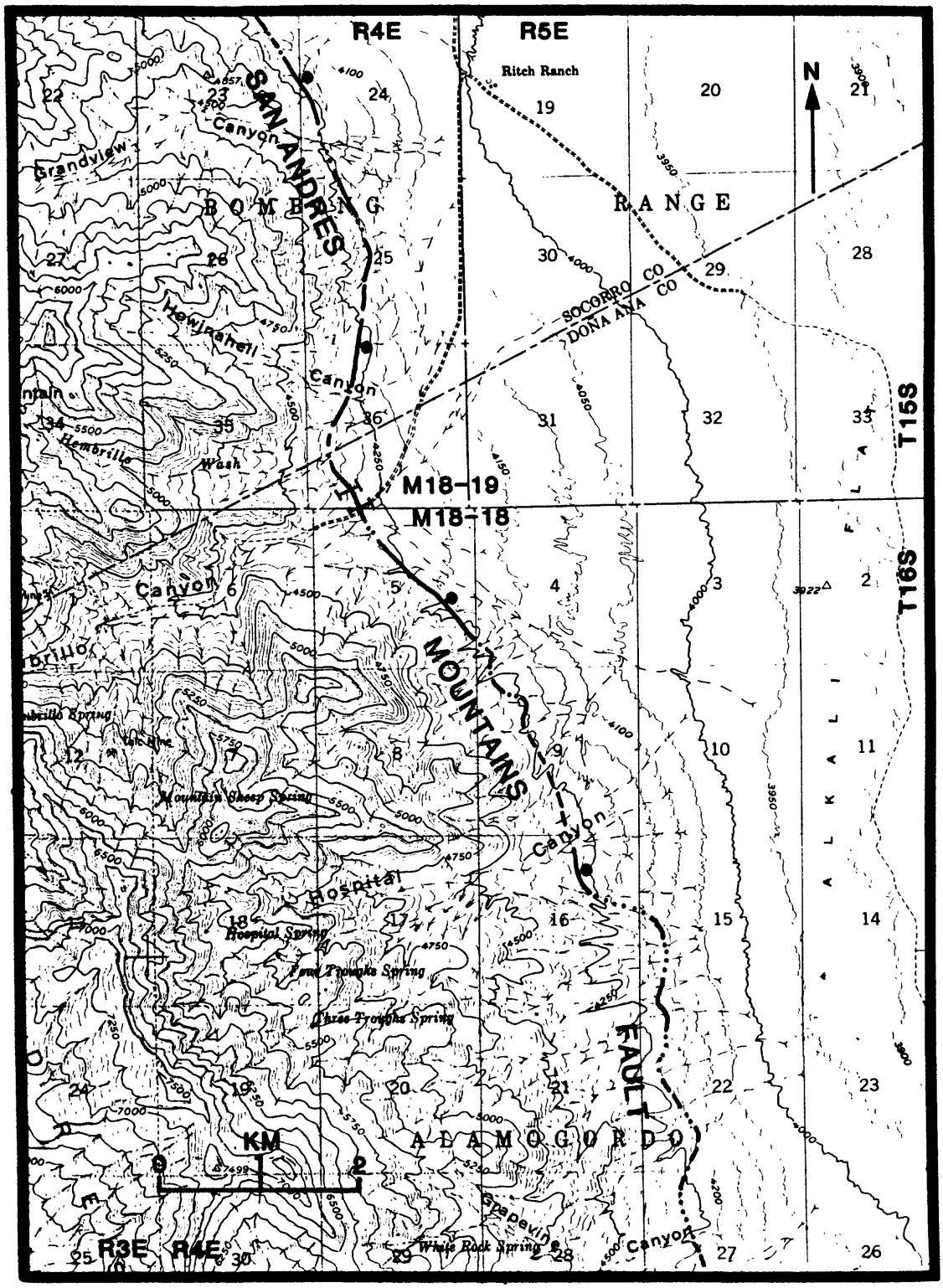

FIGURE 7.--Map showing location of scarp profiles along the north part of the central segment of the San Andres Mountains fault. Area includes northeast part of the Kaylor Mountain 15-minute quadrangle, New Mexico.

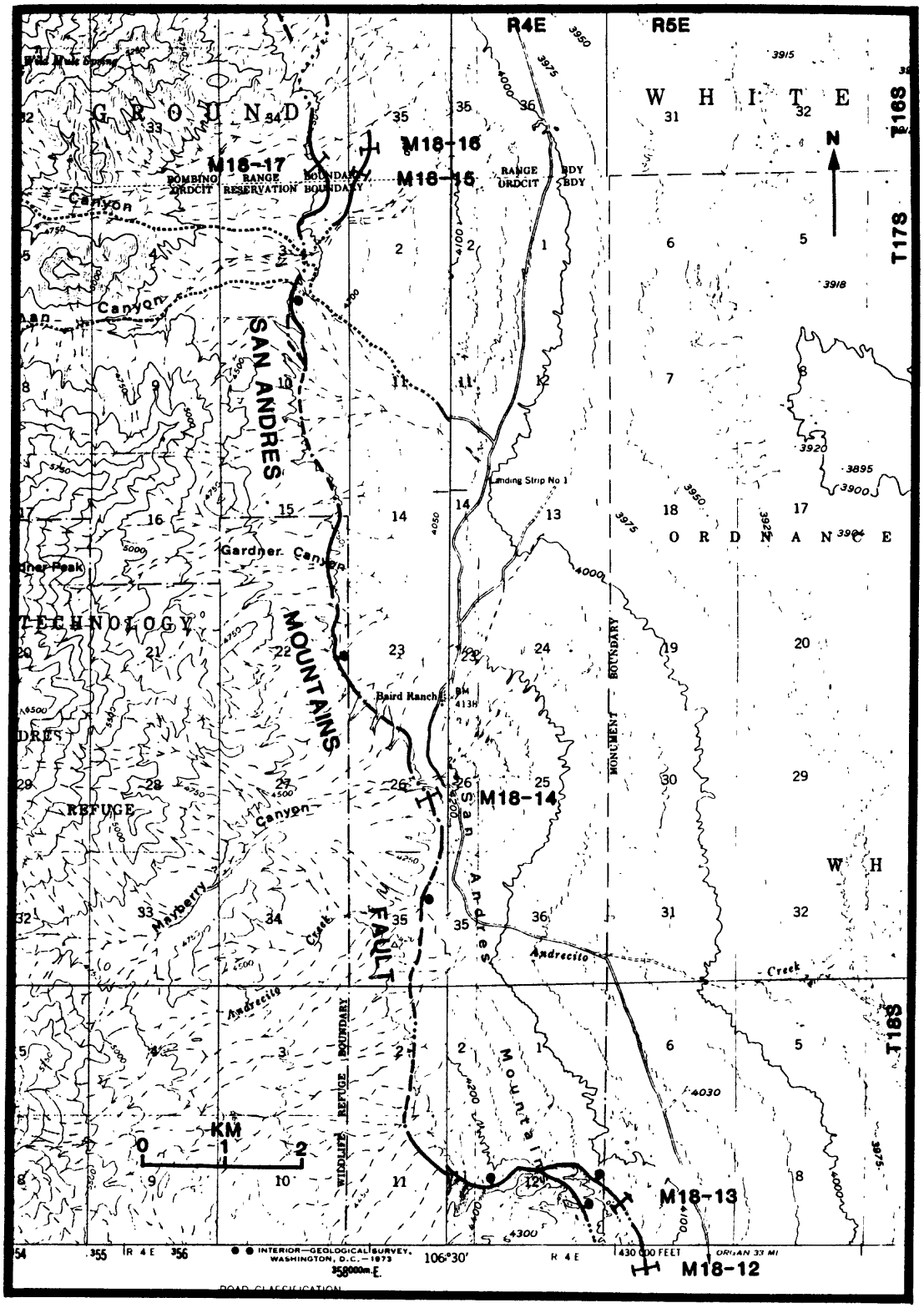

FIGURE 8.--Map showing location of scarp profiles along the south part of the central segment of the San Andres fault. Area includes parts of the Kaylor Mountain and Point of Sands 2 15-minute quadrangles, New Mexico.

The central segment extends from this point north about 48 km to Rhodes Canyon, whereas the southern segment extends about 36 km to the south and ends somewhere near Highway 70. The stratigraphic and scarp-morphology data summarized in figures 9 and 12 are for the central and southern segments of the fault, respectively.

Fault scarps along the central segment of the San Andres Mountains fault are morphologically intermediate in comparison to the northern segment (greatly eroded) and the southern segment (fresh appearing, continuous, and steeper slope angles). Four profiles across faulted late Pleistocene (Picacho) alluvium show scarp heights (Hs) of 2.7-5.4 (table 1). These scarps plot below the 15-ka control line and suggest that the most recent faulting was older than 15 ka (perhaps 25-35 ka?; fig. 9). Profiles of across late to late middle Pleistocene alluvium suggest multiple-event scarp heights of 6-15 m and total scarp heights of as much as 26-29 m. If one assumes that scarp height is greater than net surface offset (S, figs. 2 and 4), owing to backtilting and formation of grabens, then 2-4 m might be a reasonable estimate of the average offset during a major surface-faulting event (**M** 7-7.5 earthquake) on this segment of the San Andres Mountains fault. If this is the case, then the fault scarps in the Picacho alluvium may record 2-5 faulting events and those on the Tortugas may record as many as 10 faulting events. These relations suggest recurrence intervals of about 20 ka ($\leq$5 events in 100±20 ka, and $\leq$10 events in 200±50 ka). The estimated time since the most recent event (>15 ka, probably 25-35 ka) suggests that most or all of an average recurrence interval has elapsed without renewed movement on the fault.

The southern segment of the San Andres Mountains fault is distinquished by fresh-appearing fault scarps and nearly continuous surface rupturing (that is, a smaller degree of dissection by streams; figs. 10 and 11). Morphological data from five of the smaller scarps (2.8-4.8 m; table 1 and fig. 12) on late Pleistocene alluvium (Picacho and perhaps Isaacks Ranch) plot between the 5-ka and 15-ka control lines (fig. 12) and suggest that the most recent faulting event was in the early Holocene or perhaps the latest Pleistocene. Data from the larger scarps, which record several faulting events (Hm 3.7-11.2 m, table 1), plot close to the 15-ka line. These two relations suggest that the most recent faulting event on the southern segment of the San Andres Mountains fault occurred in the early Holocene or latest Pleistocene (10±5 ka), and thus is clearly younger than movement to the north. Using an average offset of 3 m per event (see previous discussion) results in an estimated (average) recurrence interval of about 20 ka for the southern segment of the San Andres Mountains fault.

The morphometric data from the youngest element of the scarps (Hs) suggests that scarps along the central segment are probably of late Pleistocene age, whereas those of the southern segment are probably of early Holocene or latest Pleistocene age (figs. 9 and 12). Scarp-morphology data from the two segments lie in distinctly different fields when plotting either Hs versus θ or Hm versus θ (figs. 6). Thus, on the basis of limited reconnaissance, there is fairly compelling evidence of at least three segments for the San Andres Mountains fault (table 2). Careful analysis of a more

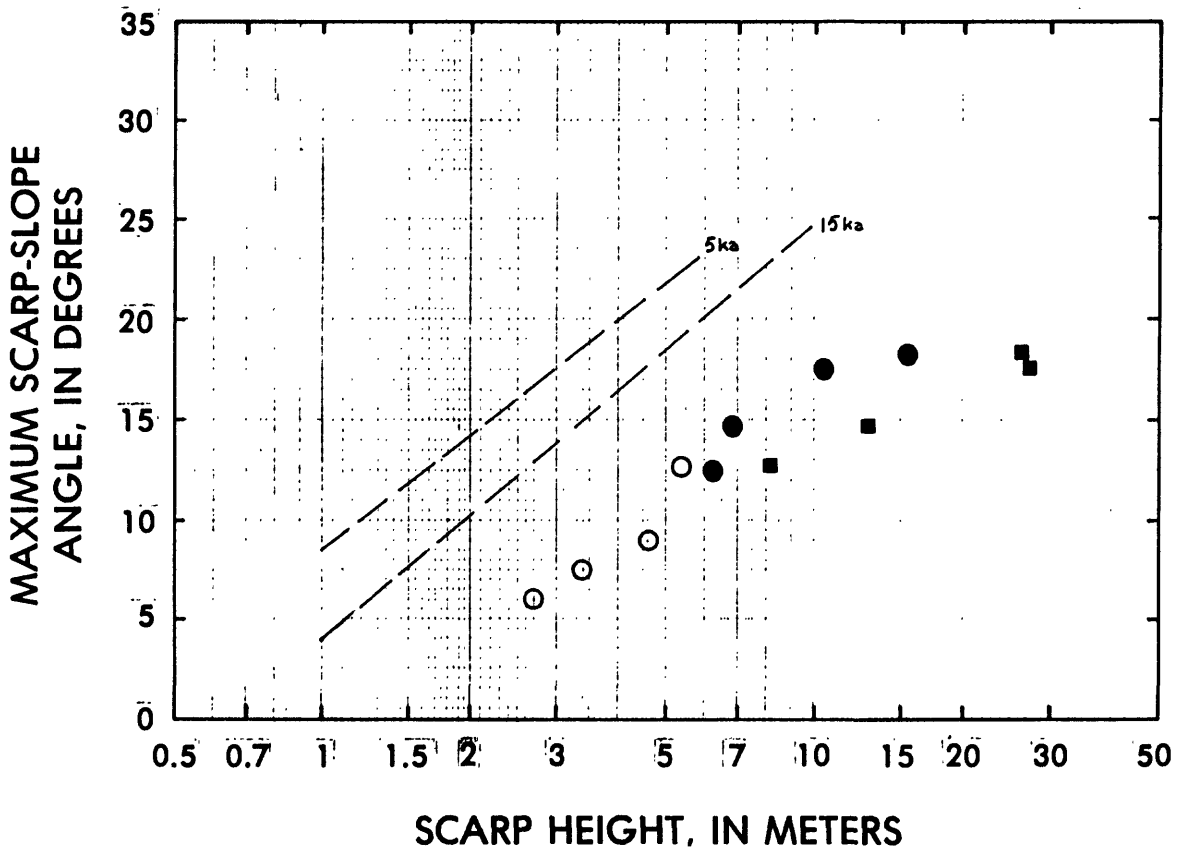

FIGURE 9.--Maximum scarp-slope angle (θ) plotted against scarp height for the central segment of the San Andres Mountains fault. Open circles are for most recent, single-event part of scarp (Hs); filled circles are for multiple-event scarp where compound (Hm); and filled squares are for total scarp height (Ht). See table 1 for morphometric data.

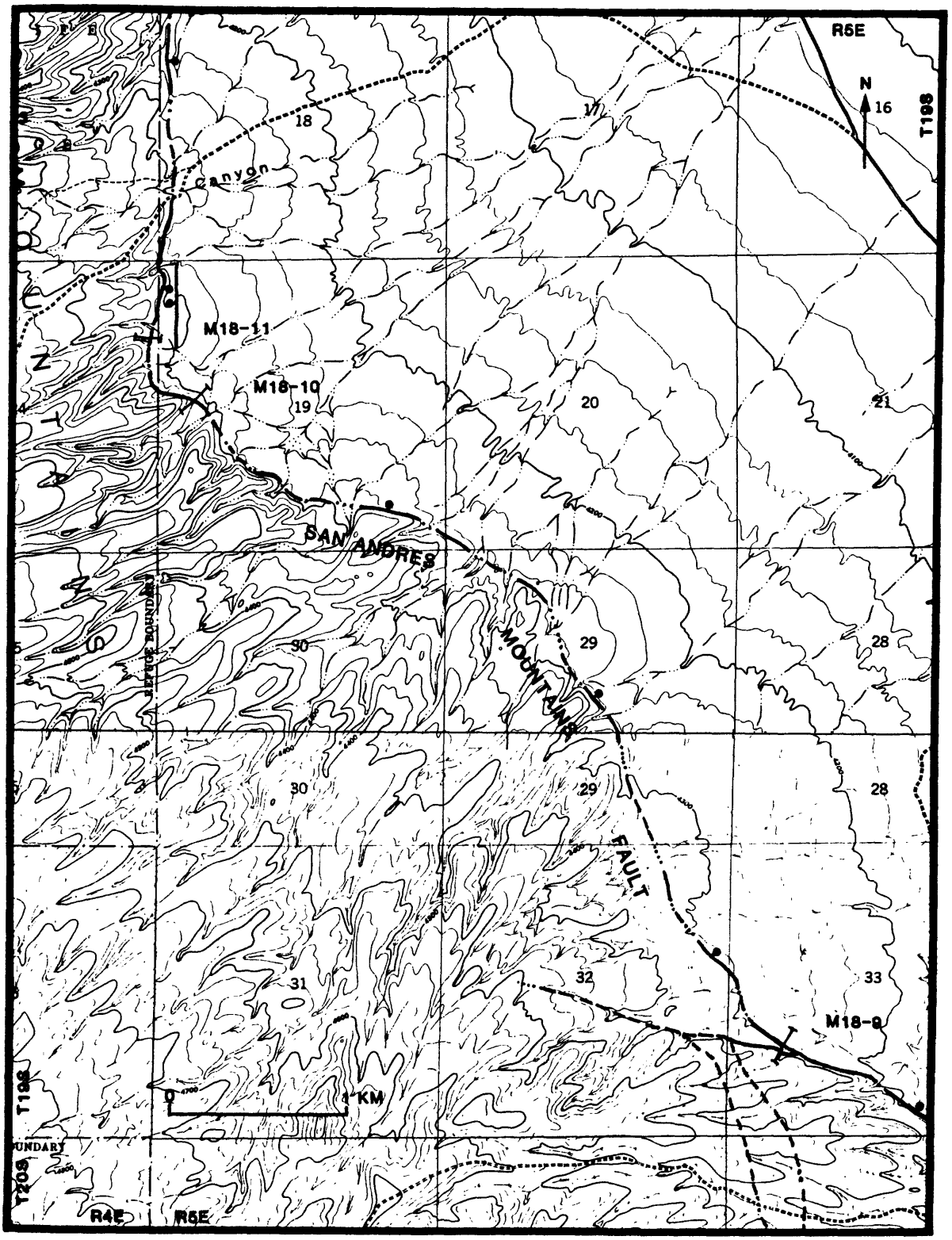

FIGURE 10.--Map showing location of scarp profiles along the north part of the southern segment of the San Andres Mountain fault. Area includes parts of the Lake Lucero and Lake Lucero SW 7.5-minute quadrangles, New Mexico.

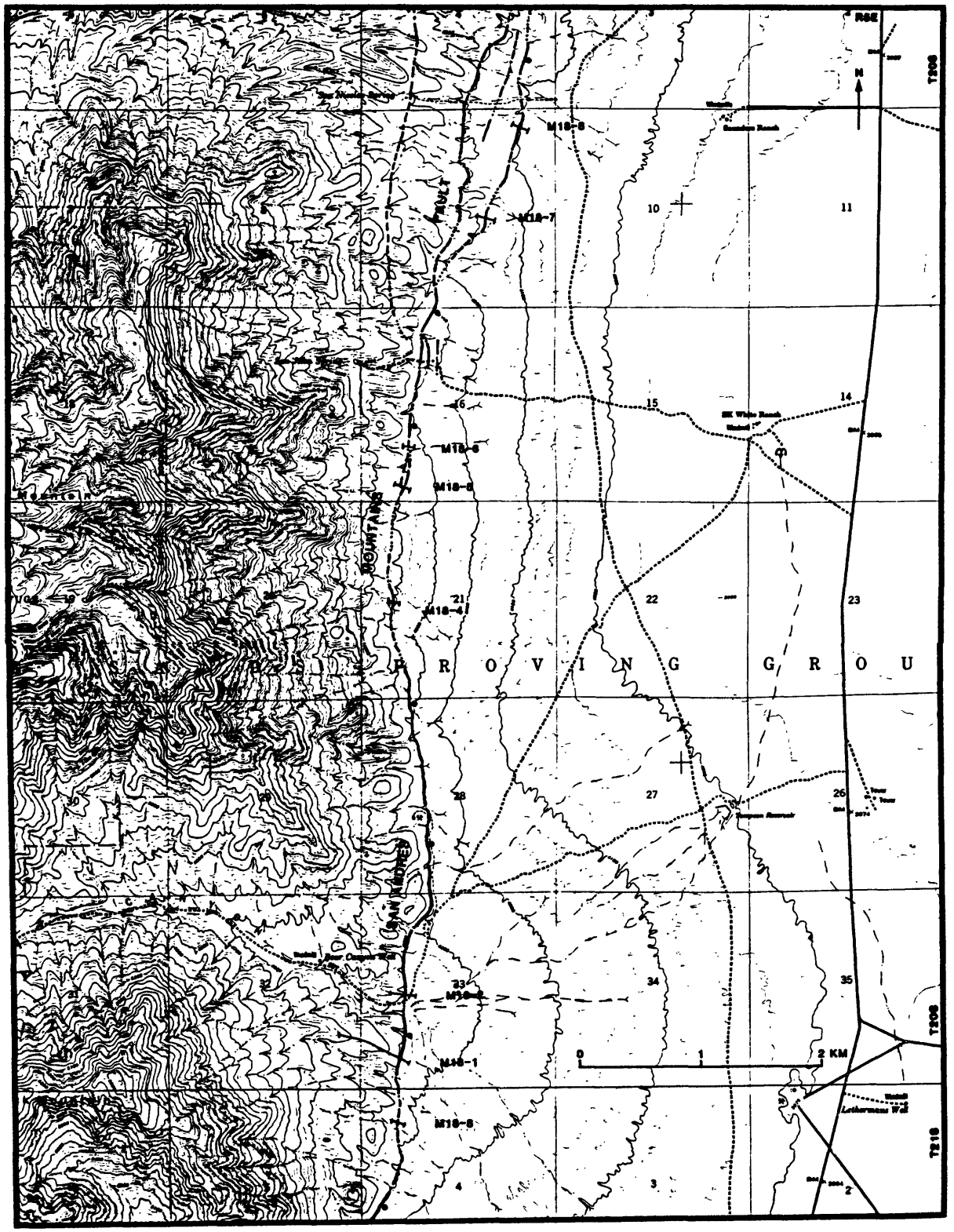

FIGURE 11.--Map showing location of scarp profiles along the south part of the southern segment of the San Andres Mountains fault. Area includes part of the Lake Lucero SW 7.5 minute-quadrangle, New Mexico.

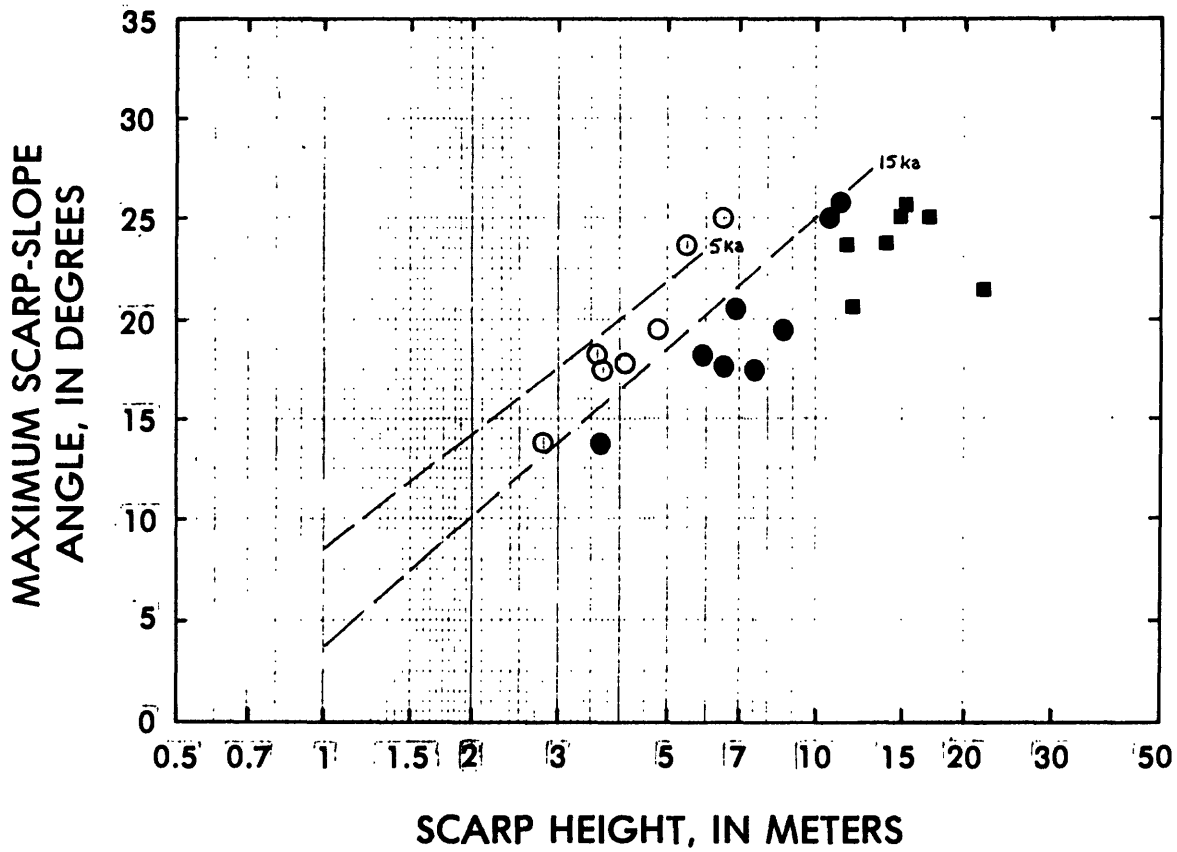

FIGURE 12.--Maximum scarp-slope angle (θ) plotted against scarp heights (Hs, Hm, and Ht) for the southern segment of the San Andres Mountains fault. Open circles are for most recent, single-event part of scarp; filled circles are for multiple-event scarp where compound, and filled squares are for total scarp height. See table 1 for morphometric data.

complete collection of scarp-morphology data, detailed mapping of surficial deposits along the fault, and excavation of trenches at selected localities along the fault would help substantiate the segmentation proposed here.

Organ Mountains Fault

The Organ Mountains fault (no. 4, fig. 1 and table 2) extends 42 km along the eastern margin of the Organ Mountains from New Mexico State Highway 70 southward to Anthony Gap, at the north end of the Franklin Mountains. The fault separates the Tularosa Basin on the east from the Organ Mountains on the west. The fault is marked by a series of prominent fault scarps in alluvium of Holocene to middle Pleistocene age. Bedrock generally is not exposed at the fault, but is probably buried on the upthrown block by a relatively shallow cover of surficial deposits (see Seager's 1981 cross sections).

About 8 km south of White Sands, N. Mex., the Artillery Range fault splays eastward off the Organ Mountains fault. The Artillery Range fault (no. 5, fig. 1 and table 2) is concave to the west and shows evidence of late Pleistocene movement farther south than does the Organ Mountains fault. The Artillery Range fault shows evidence of Holocene movement (Seager, 1981) and has characteristics (for example, direction and amount of dip, sense of movement) similar to the Organ Mountains fault. The northern part of the Artillery Range fault is marked by several en echelon faults that trend north-northwest. Farther south the trace of the fault trends southwestward and is obscured by bolson fill, but it merges with the Organ Mountains fault. From this point southward, evidence for the timing of movement on the Organ Mountains fault is sparse although Seager (1981) shows the fault cutting young (late Quaternary) piedmont alluvium.

The prominent fault scarps along the east side of the Organ Mountains were first mentioned by Reiche (1938). However, details of the Quaternary history of the Organ Mountains fault have been largely decipered by Gile (1986, 1987) from exposures of soils and alluvium, stratigraphic relations, and fault scarps in the area between the Cox Ranch (also known as the Augustine Ranch) and Texas Canyon (fig. 13). (This area is about 3-4 km west-southwest of White Sands, N. Mex.) Scarp-morphology data along the fault in this area (fig. 14) suggest that that most recent movement occurred in middle Holocene time (Hs data plot close to the 5-ka control line). However, Gile's (1986) soil studies in this area and suggests that the most recent faulting is <2 ka and perhaps as young as 1 ka. The single-event scarps in late Holocene alluvium are less than 2 m high, whereas multiple event scarps in older Holocene alluvium are 3.5 to 5.8 m high (table 1). Just south of the Cox Ranch, fault scarps on the Isaacks Ranch(?) and Picacho alluviums of Kottlowski and Hawley (1969) are 9.9-15.5 high and definitely compound.

Elsewhere along the fault, scarp heights range from 1.5 to 30 m in coarse grained alluvial-fan deposits. From these relations it is clear the the Organ Mountains fault (and from similar relations the associated Artillery Range fault) has had a long history of repeated movement. In addition, Gile's studies, and my scarp-morphology data (fig. 14) indicate two major surface

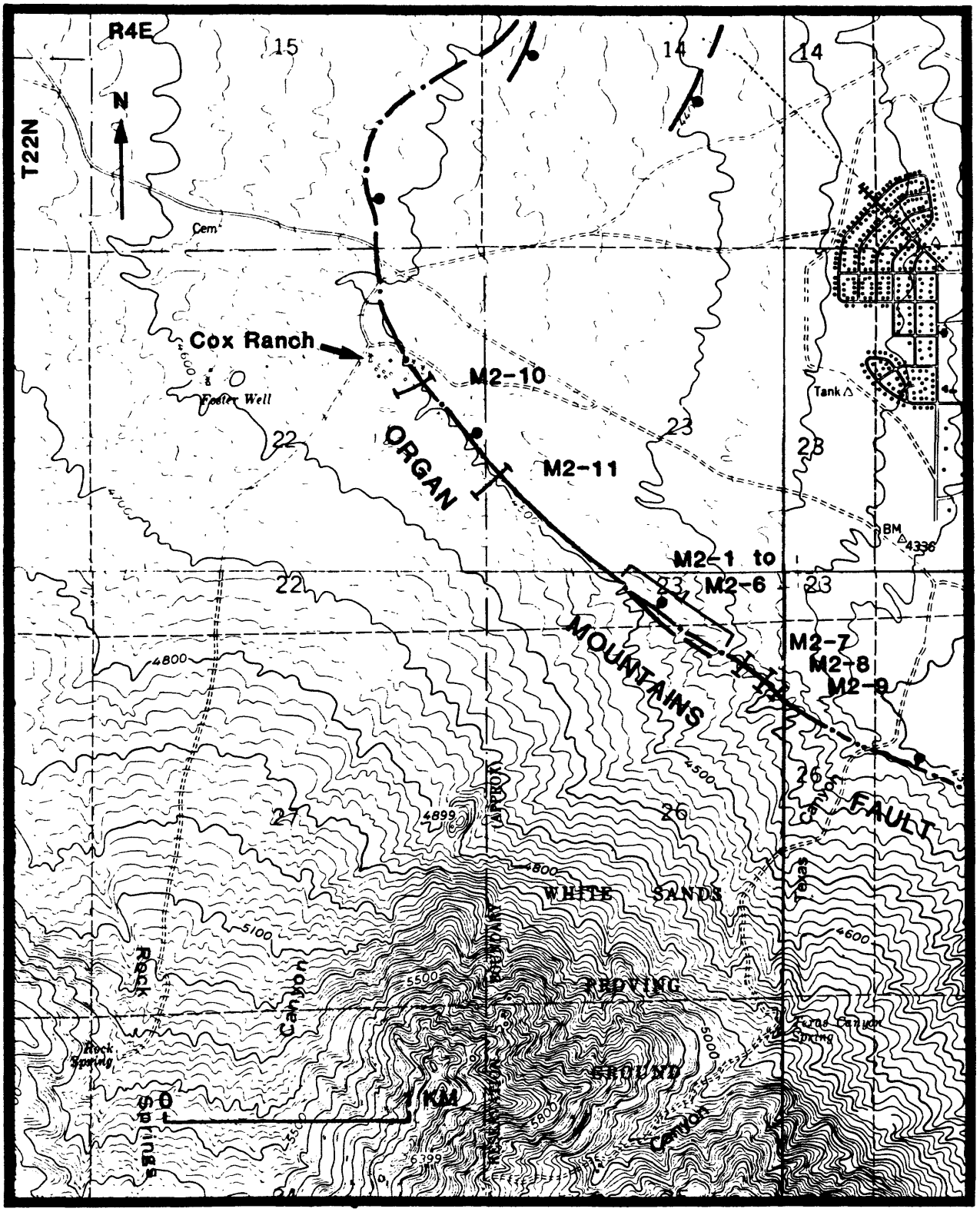

FIGURE 13.--Map showing location of scarp profiles along the Organ Mountains fault. Area includes parts of the Organ and Organ Peak 7.5-minute quadrangles, New Mexico.

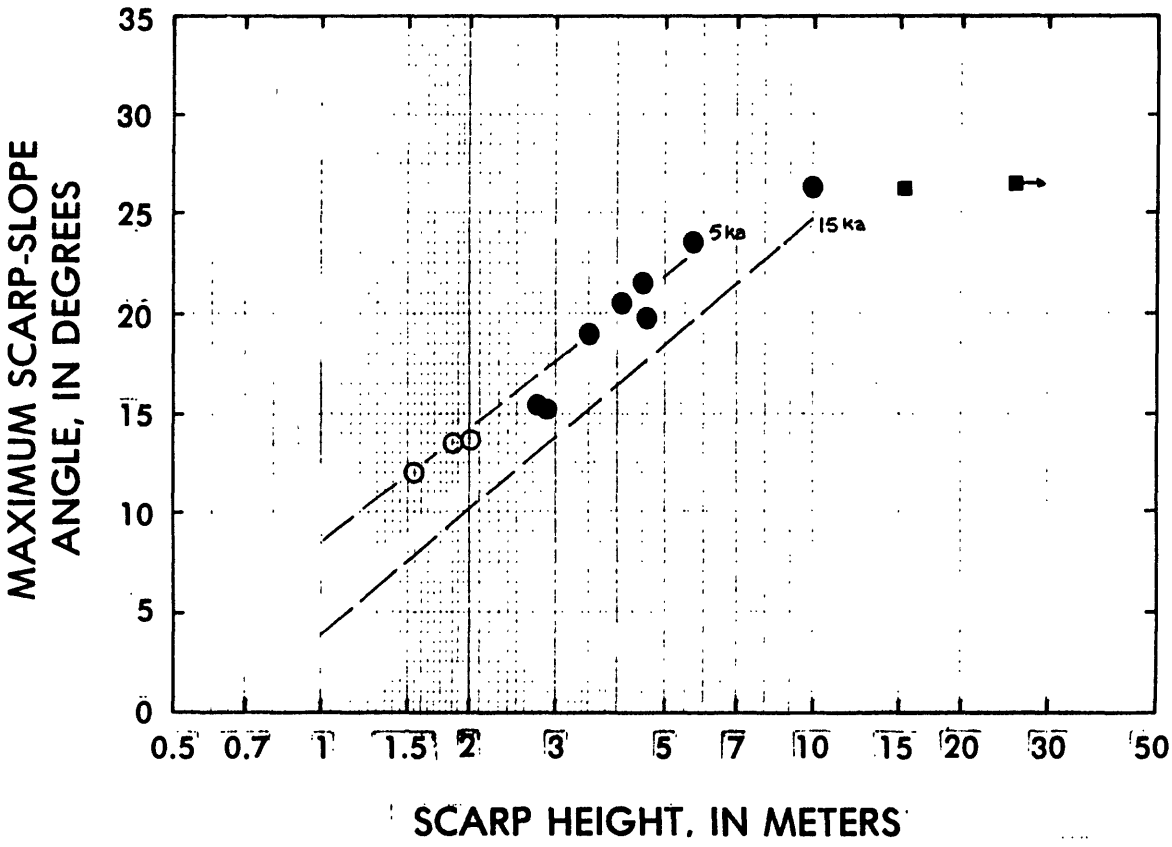

FIGURE 14.--Maximum scarp-slope angle (θ) plotted against scarp heights (Hs, Hm, and Ht) for the southern segment of the Organ Mountains fault (2). Open circles are for most recent, single-event part of scarp; filled circles are for multiple-event scarp where compound, and filled squares are for total scarp height. See table 1 for morphometric data.

faulting events in the Holocene. Seager (1981) argues that in the past 5 ka about 10 m of offset has occurred, although our profile data suggests maximum scarp heights of 6 m in the Organ alluvium (middle to upper Holocene).

East Franklin Mountains Fault

The East Franklin Mountains fault (no. 6, fig. 1 and table 2) extends from near Anthony Gap (about 16 km east of La Mesa, N. Mex.), which marks the northern end of the Franklin Mountains, southward along the Franklin Mountains 45 km to the International Boundary at El Paso, Tex. The fault is here named for its prominent trace along the east side of the Franklin Mountains. This fault was first mapped by Richardson (1909), and latter studied by Sayre and Livingston (1945). Lovejoy and Seager in 1978 (p. 68-69) suggested that this fault, as well as the uplift of the Franklin Mountains, was caused by compression of the crust and high-angle reverse faulting on both sides of the range. In a later study, however, Seager (1980, p 133) argues that Cenozoic motion on the fault was caused by tensional forces, resulting in the formation of a major high-angle normal fault (the San Andres-Organ-East Franklin Mountains fault system of this report). This latter interpretation is in agreement with other structural data collected in the area since 1978.

The southern half of the fault zone has been largely obscured by housing and light construction, and although the fault scarp can be traced through El Paso to the International Border with Mexico on the basis of abrupt topographic escarpments, there is little evidence of its time of most recent movement. Sayre and Livingston (1945, p. 34-35, 46) measured 125 m (410 ft) of displacement in Quaternary deposits (Camp Rice Formation) near William Beaumont Hospital in northeast El Paso. However, fault scarps are still excellently preserved in the Fort Bliss Military Reservation north of El Paso, particulary in the Castner Range near Fusselman Canyon (fig. 15). Nineteen scarp profiles were collected in the Castner Range: 12 from south of the Trans Mountain Highway (375) and 7 from the area north of the highway.

Scarp heights along the East Franklin Mountains fault are typically less than the amount of surface offset owing to extensive alluvial deposition at the toe of scarps. For example, profiles m17-1 and m17-2 (fig. 15) are on alluvial surfaces locally known as the Gold Hill and Kern Place, respectively (Picacho and Tortugas equivalents of Hawley and Kottlowski, 1969). These two scarps are 9.3 and 12.4 m high, but both are partly buried by alluvium of latest Pleistocene and Holocene age (Isaacks Ranch and Organ alluvium of Hawley and Kottlowski, 1969). About 1 km south of Fusselman Canyon, profile m17-4 was measured across Isaacks Ranch (or perhaps younger) alluvium. This scarp is 3.7 m high and may reflect the youngest movement on the fault. Single-event scarp heights (Hs) from large scarps are typically 3-5 m, so the 3.7-m height recorded at m17-4 seems reasonable for a single, not multiple faulting event. The scarp-morphology data (Hs versus θ, fig. 16) suggest that the youngest scarps along the East Franklin Mountains fault are early Holocene or latest Pleistocene in age (10±5 ka).

Late to late middle-Pleistocene alluvial-fan deposits (Gold Hill and Kern Place alluvium of Kottlowski, 1958) have multiple-event scarps that vary in height according to their depositional setting. Scarps along the main fault may be as high as 9-12 m, whereas minor faults and splays from the main fault

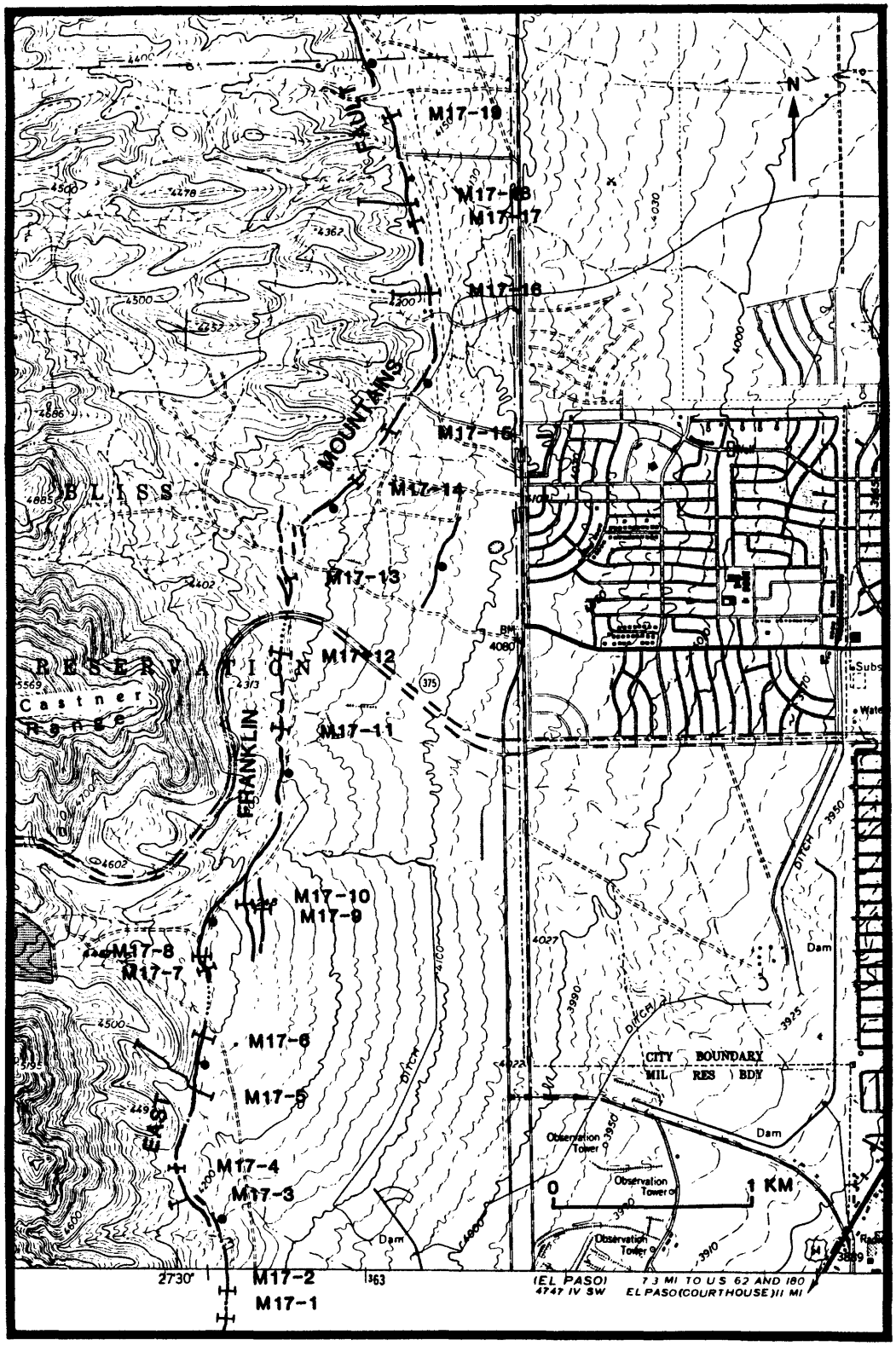

FIGURE 15.--Map showing location of scarp profiles along the East Franklin Mountains fault in the Castner Range of the Fort Bliss Military Reservation. Area includes the southeast part of the North Franklin Mountain 7.5-minute quadrangle, Texas.

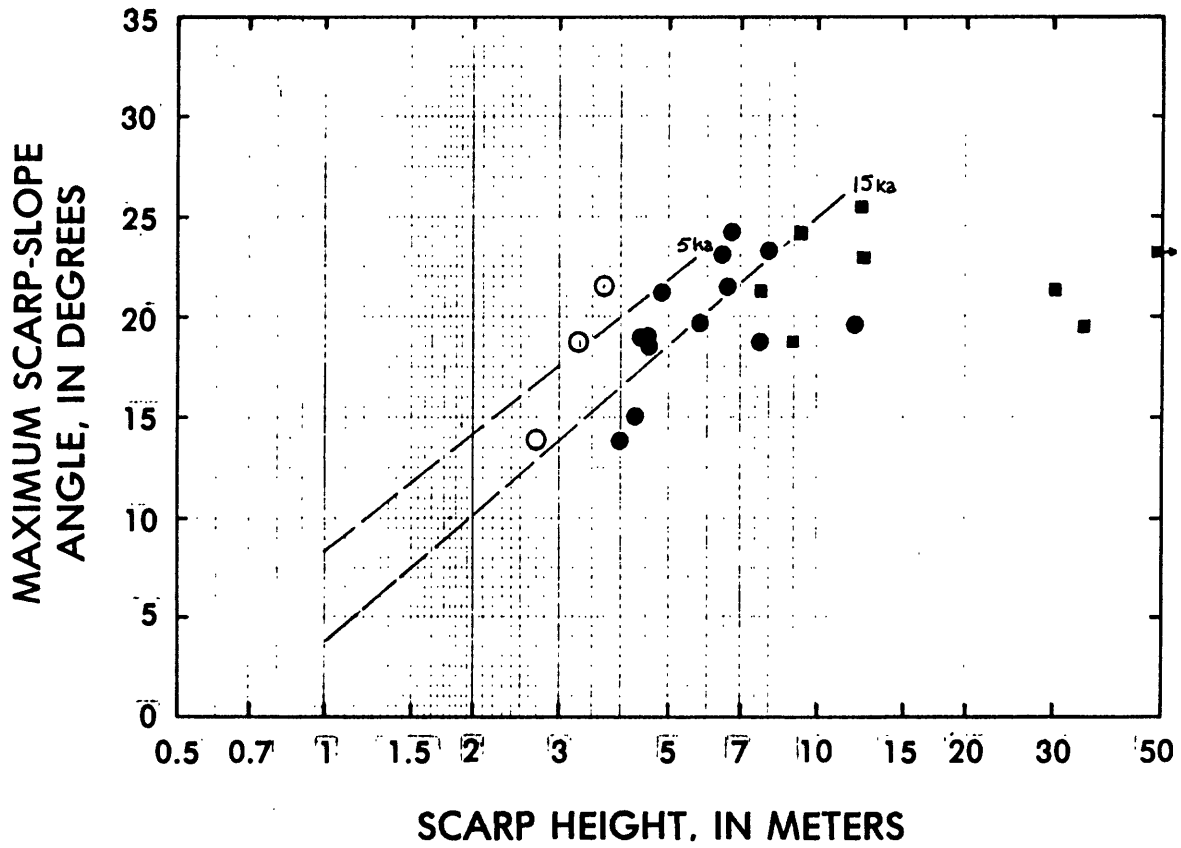

FIGURE 16.--Maximum scarp-slope angle (θ) plotted against scarp height for the southern segment of the East Franklin Mountains fault (3). Open circles are for most recent, single-event part of scarp (Hs); filled circles are for multiple-event scarp where compound (Hm); and filled squares are for total scarp height (Ht). See table 1 for morphometric data.

have scarps that are smaller (2-4 m). Although scarps on the Jornada I and Jornada II surfaces (middle Pleistocene) are 30-60 m in height, they are steepest near the base of the scarp, which suggests substantial burial of the downdropped fault block. Scarps in basin-fill deposits of the Camp Rice Formation are typically >60 m, and may locally reach 125 m in height.

Pre-Holocene alluvial deposits along the east side of the Franklin Mountains record a long history of faulting. Scarps with compound angles are commonly 4-12 m high, but larger scarps also show some evidence of compound angles (for example, profiles m17-5, m17-16, and m17-18; table 1). The 30-35 m scarps probably record offset of the Jornada I surface (about 350±50 ka) and the one 60-m-high scarp (m17-5) probably records offset of the constructional surface of the Camp Rice Formation (lower La Mesa surface at Las Cruces, about 500 ka; age estimates from Machette, 1985, fig. 8). These two offset surfaces yield minimum slip rates of 0.08-0.10 mm/yr for the past 350 ka and about 0.12 mm/yr for the past 500 ka. These rates are surprisingly close to the value of 120 m/m.y. (0.12 mm/yr) suggested by Lovejoy and Seager (1978, p. 68).

Alamogordo Fault (New Name)

Both Otte (1959) and Pray (1961) recognized the importance of the major range-bounding fault that lies at the base of the Sacramento Mountains just east of Alamogordo. This fault is here named the Alamogordo fault (no. 7, fig. 1 and table 2); it separates the strongly uplifted Sacramento Mountains from the deep sediment-filled Tularosa Basin. The surface trace of the fault is conspicuous for 57 km, from 7 km north of Tularosa, south to Bug Scuffle Canyon, which is about 30 km south of Alamogordo, N. Mex. The fault splays at its northern end (Weir, 1965): the eastern branch is inferred to extend an additional 32 km northeast along a reentrant of the Sacramento Mountains, through Three Rivers, New Mexico, and along the western edge of the Phillips Hills. The western branch is thought to extend 22 km northwest, where it is buried beneath the alluvial cover of the Tularosa Basin (Weir, 1965). Neither of these extensions of the fault record movement in late middle-Pleistocene (several 100 ka) or younger deposits. At the southern end of the fault, south of Bug Shuffle Canyon, the fault turns southwest and extends along Pipeline Canyon as a moderately dissected scarp.

Stratigraphic throw on the Alamogordo fault is as much as 2.3 km east of Alamogordo, but decreases to the north and south (Pray, 1961). Otte (1959) discusses evidence for abundant Pleistocene displacement along the Alamogordo fault, including the presence of "piedmont" scarps up to 7 m in height and isolated gravel cappings (deposits) that are 30-60 m above the present drainage.

Scarp-morphology data was collected at two localities along the Alamogordo fault. Eight profiles were measured on the northeast edge of Alamogordo just south of the International Space Hall of Fame and New Mexico State University campus (fig. 17, profiles m30-1 to m30-8; table 1). An additional six profiles were measured across alluvial fans at the mouths of major stream canyons southeast of Alamogordo (fig. 18, profiles m31-1 to m31-6; table 1). These data indicate that the scarps east and southeast of Alamogordo are either early(?) Holocene or latest Pleistocene. I found two scarps that are 2-2.9 m high, whereas most others are greater than 4 m high. This relation

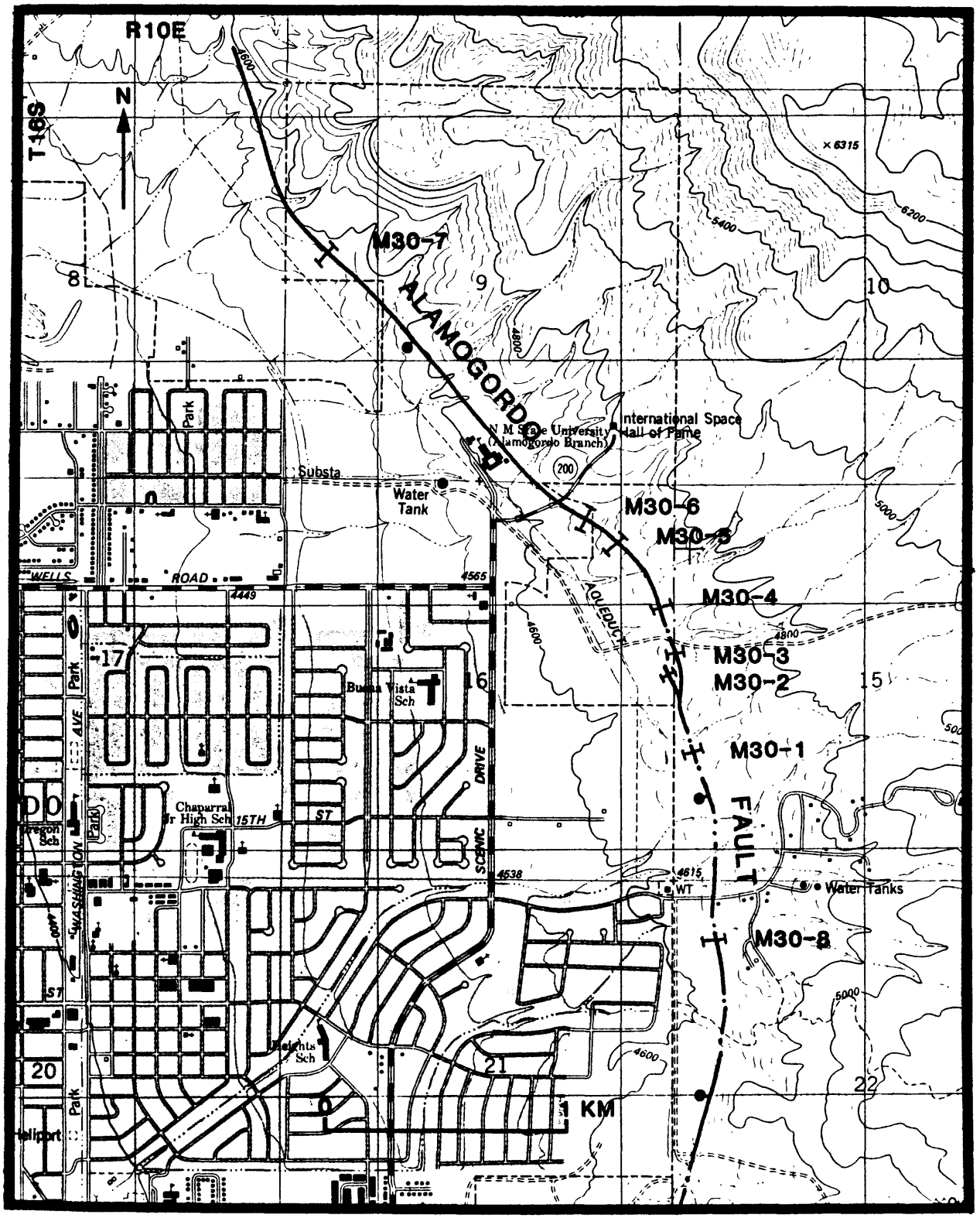

FIGURE 17.--Map showing location of scarp profiles along the Alamogordo fault, east of Alamorgo, New Mexico. Area includes part of the Alamogordo 7.5-minute quadrangle, New Mexico.

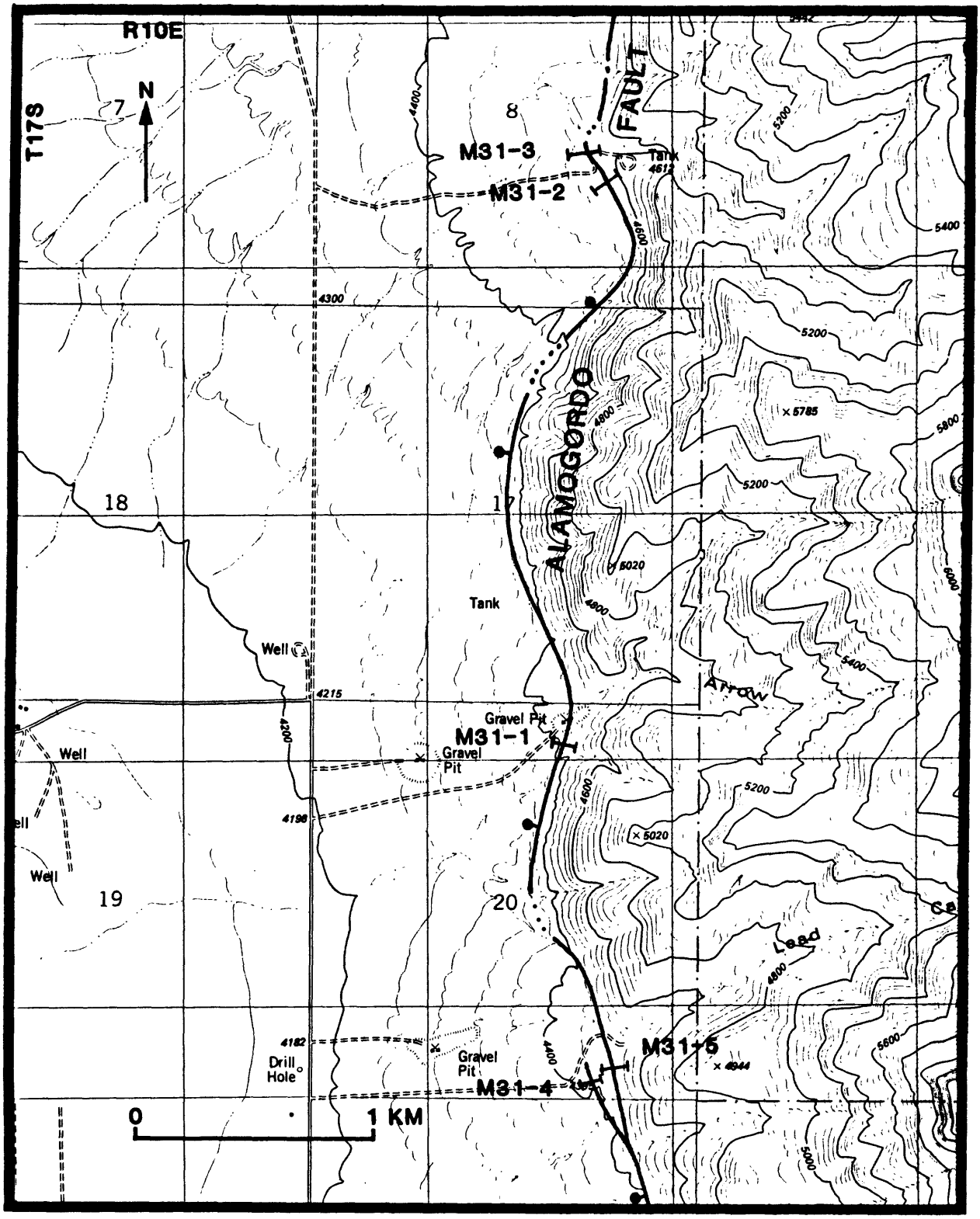

FIGURE 18.--Map showing location of scarp profiles along the Alamogordo fault, southeast of Alamogordo, New Mexico. Area includes part of the Mule Peak 7.5-minute quadrangle, New Mexico.

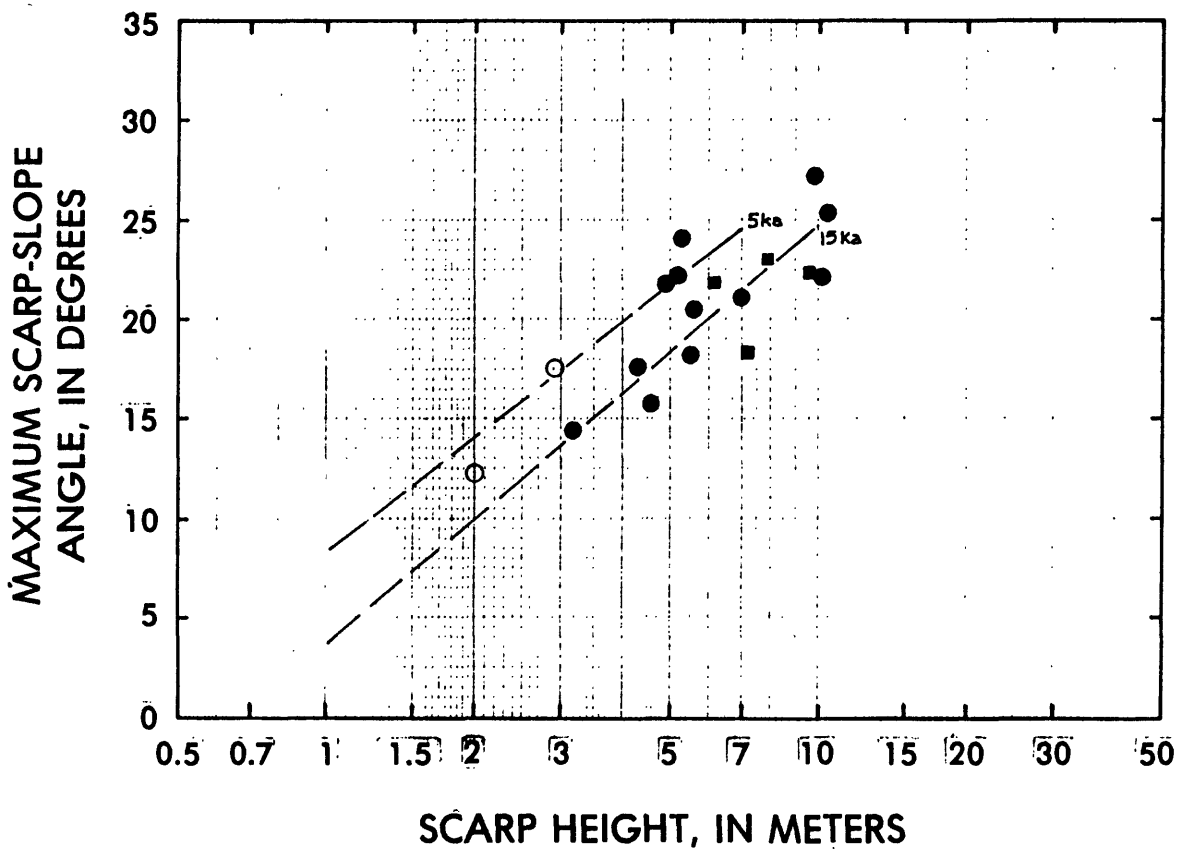

FIGURE 19.--Maximum scarp-slope angle (θ) plotted against scarp heights for the Alamogordo fault). Open circles are for most recent, single-event part of scarp (Hs); filled circles are for multiple-event scarp where compound (Hm); and filled squares are for total scarp height (Ht). See table 1 for morphometric data.

and the fact that the small scarps plot near the 5-ka line in fig. 19, suggest the fault may have had two episodes of movement in the Holocene and latest Pleistocene (past 35 ka). Although I concentrated on fault scarps in fan-head alluvium (generally late Pleistocene and Holocene), large scarps are preserved in older alluvium all along the fault. Because the age and heights of these scarps remain undocumented, average values for slip rates and recurrence intervals cannot be calculated. However, I suspect that the Alamogordo fault has a history of Quaternary movement much like the East Franklin Mountains fault and the central segment of the San Andres Mountains fault.

INTRABASIN FAULTS

The southern part of the Tularosa Basin and most of the Hueco Basin near El Paso (fig. 1) are riddled with seemingly young fault scarps that cut the surface of the ancient constructional basins. Seager (1980, fig. 2) mapped these faults and describes their possible origin as a response to down warping of basin-fill sediments caused by localized extension beneath the western side of the basins. Many of the intrabasin faults may be shallow-seated features; however, some of the more continuous ones may penetrate rather deep and be capable of generating earthquakes.

The most continuous of the intrabasin faults are at least 30 km long and perhaps as much as 35 km long. However, many of them are only 5-10 km long and join one another to form long or broad en echelon zones of surface faulting. The height of scarps along the intrabasin faults is typically 3-7 m, although some are as large as 20 m (Seager, 1980, found some as much as 28 m high). The faults are post-middle Pleistocene (they cut near-surface deposits of the Camp Rice Formation), but the youngest movement could be late Pleistocene or younger. A thick blanket of Holocene eolian sand is draped across the fault scarps in the Hueco Basin, such that their morphology is greatly subdued. Reconnaissance in this area failed to uncover exposures of the intrabasin faults, nor reveal evidence of their recency of movement. An extensive program of deep trenching would be needed to establish more details about their time of last movement.

SUMMARY

Evidence of Quaternary faulting is abundant in the southern part of the Rio Grande rift of south-central New Mexico. In the vicinity of WSMR, major faults offset Pliocene to early(?) Pleistocene basin-fill deposits and middle to latest Pleistocene and Holocene surficial deposits. Morphologic, pedologic (soils), and geologic data collected along the major faults in and near WSMR, New Mexico, show that all were active during the late (130-10 ka) or latest (35-10 ka) Pleistocene, and four faults or fault segments were probably active in the Holocene (less than 10 ka). These faults are the southern segment of the San Andres fault, the Organ Mountains fault, the East Franklin Mountains fault, and the Alamogordo fault. Data from the Cox Ranch site on the Organ Mountains fault suggest two discrete movements in the past 5 ka, making it the most active of the Quaternary faults in the region. This site is immediately west of White Sands, New Mexico--the headquarters for WSMR. In addition to these faults, I suspect that the central and northern segments of San Andres fault have latest Pleistocene and late Pleistocene movement, respectively.

The late Pleistocene and Holocene faults in WSMR have evidence of segmentation (from comparisons of scarp-morphology data) and recurrent movement. The lengths of these faults and fault segments range are commonly 36-57 km (except for the 22-km-long less active northern segment of the San Andres Mountain fault). This length of faulting, coupled with evidence of about 2 m of displacement per surface-faulting events, is compatible with earthquakes of moment-magnitude 7-7.5 as seen historically in the Basin and Range province. The average recurrence interval for large-magnitude earthquakes at WSMR is probably about 2,000 yr, as determined from evidence of five surface-rupturing events (on four faults and fault segments) during the past 10,000 yrs (Holocene) at or near WSMR. Recurrence intervals for surface ruptures on individual faults ranges from 4,000-5,000 yrs on the Organ Mountains fault to 20,000 yrs on the southern and central segments of the San Andres Mountains fault.

Large fault scarps (25-50 m high) are preserved on middle to upper Pleistocene surficial deposits along the San Andres, Organ Mountains, and East Franklin Mountains faults. Scarps this large are the result of recurrent faulting, as evidenced by decreasing amounts of offset in progressively younger deposits. Although created by faulting, some of the relief on these escarpments (fault-line scarps) may be the result of erosion, whereas as much as half of the offset on the fault may be masked by younger deposits that accumulate at the toe of a fault scarp. Thus, the scarp heights recorded herein may not accurately reflect offset along the fault system.

Intrabasin faults are present in the Tularosa Basin south of White Sands, N. Mex., and particularly abundant in the Hueco Basin northeast of El Paso, Tex. The times of movement on these faults are largely unknown owing to an extensive cover of eolian sand. However, their youthful expression and undissected nature suggest that they may be of late Pleistocene age.

REFERENCES

Aldrich, M.J., and Laughlin, A.W., 1982, Orientation of least-principal horizontal stress: Arizona, New Mexico, and the Trans-Pecos area of West Texas: Los Alamos National Laboratory Publication LA-9158-Map UC-11, scale 1:1,000,000.

Bachman, G.O., and Mehnert, H.H., 1978, New K-Ar dates and the late Pleistocene to Holocene geomorphic history of the central Rio Grande region, New Mexico: Geological Society of America Bulletin v. 89, p. 283-292.

Baldridge, W.S., Bartov, Y., and Kron, A., 1983, Geologic map of the Rio Grande rift and southeastern Colorado Plateau, New Mexico and Arizona, in Riecker, R.E., ed., Rio Grande rift--tectonics and magmatism: Washington, D.C., American Geophysical Union, 2nd printing (1982), scale 1:500,000.

Birkeland, P.W., 1984, Soils and Geomorphology: New York, Oxford University Press, 372 p.

Bucknam, R.C., 1980, Characteristics of active faults in the Great Basin, in Summaries of Technical Reports, v. 9, National Earthquake Hazards Reduction Program: U.S. Geological Survey Open-File Report 80-6, p. 94-94.

Bucknam, R.C., and Anderson, R.E., 1979, Estimation of fault-scarp ages from a scarp-height-slope-angle relationship: Geology, v. 7, no. 1, p. 11-14.

Chapin, C.E., 1979, Evolution of the Rio Grande rift--a summary, in Riecker, R.E., ed., Rio Grande rift--tectonics and magmatism: Washington, D.C., American Geophysical Union, p. 1-5.

Chapin, C.E., Chamberlain, R.M., Osburn, G.R., Sanford, A.R., and White, D.W., 1978, Exploration framework of the Socorro geothermal area, New Mexico, in Chapin, W.E. and Elston, W.E., eds., Field guide to selected cauldrons and mining districts of the Datil-Mogollon volcanic field, New Mexico: New Mexico Geological Society Special Publication no. 7, p. 115-129.

Chapin, C.E., and Seager, W.R., 1975, Evolution of the Rio Grande rift in the Socorro and Las Cruces areas, in Seager, W.R., Clemons, R.E., and Callender, J.F., eds., Guidebook of the Las Cruces country: New Mexico Geological Society 26th Field Conference Guidebook, p. 297-321.

Cook, F.A., McCuller, D.B., Decker, E.R., and Smithson, S.B., 1979, Crustal structure and evolution of the southern Rio Grande rift, in Riecker, R.E., ed., Rio Grande rift--tectonics and magnetism: Washington D.C., American Geophysical Union, p. 195-208.

Elston, W.E., and Bornhorst, T.J., 1979, The Rio Grande rift in context of regional post-40 M.Y. volcanic and tectonic events, in Riecker, R.E., ed., Rio Grande rift--tectonics and magmatism: Washington D.C., American Geophysical Union, p. 416-438.

Fitzsimmons, J.P., 1955, ed., Guidebook to south-central New Mexico: New Mexico Geological Society Sixth Annual Field Conference Guidebook, 193 p.

Gile, L.H., 1986, Late Holocene displacement along the Organ Mountains fault in southern New Mexico--a summary: New Mexico Geology, v. 8, no. 1, p. 1-4.

_____1987, Late Holocene displacement along the Organ Mountains fault: New Mexico Bureau of Mines and Mineral Resources Bulletin 116, 43 p.

Gile, L.H., Hawley, J.W., and Grossman, R.B., 1981, Soils and geomorphology in the Basin and Range area of southern New Mexico--guidebook to the desert project: New Mexico Bureau of Mines and Mineral Resources Memoir 39, 222 p.

Hawley, J.W., compiler, 1978, Guidebook to the Rio Grande rift in New Mexico and Colorado: New Mexico Bureau of Mines and Mineral Resources Circular 163, 241 p.

Hawley, J.W., Bachman, G.O., and Manley, Kim, 1976, Quaternary stratigraphy in the Basin and Range, Southern Rocky Mountains, and Great Plains Provinces, New Mexico and western Texas, in Mahaney, W.C., ed., Quaternary stratigraphy of North America: Stroudsburg, Pa., Dowden, Hutchinson, and Ross, p. 235-274.

Hawley, J.W., and Kottlowski, F.E., 1969, Quaternary geology of the south-central New Mexico border region, in Kottlowski, F.E., and Lemone, D.V., eds., Border stratigraphy symposium: New Mexico Bureau of Mines and Mineral Resources Circular 104, p. 89-115.

Hawley, J.W., Kottlowski, F.E., Strain, W.S., Seager, W.R., King, W.E, and Lemone, D.V., 1969, The Santa Fe Group in south-central New Mexico border region, in Kottlowski, F.E., and Lemone, D.V., eds., Border stratigraphy symposium: New Mexico Bureau of Mines and Mineral Resources Circular 104, p. 52-76.

Kelley, V.C., 1955 , Regional tectonics of south-central New Mexico, in Fitzsimmons, J.P., ed., Guidebook of south-central New Mexico: New Mexico Geological Society Sixth Annual Field Conference Guidebook, p. 96-104.

Kelley, V.C., and Silver, Caswell, 1952, Geology of the Caballo Mountains, New Mexico: University of New Mexico Press Publications in Geology 4, 286 p.

Kottlowski, F.E., 1955, Geology of the San Andres Mountains, New Mexico, in Fitzsimmons, J. P., ed., Guidebook of south-central New Mexico: New Mexico Geological Society Sixth Annual Field Conference Guidebook, p. 137-145.

_____1958, Geologic history of the Rio Grande near El Paso, Texas, in Franklin and Hueco Mountains, Texas: West Texas Geological Society Field Trip Guidebook, p. 46-54.

Laughlin, A.W., Aldrich, M.J., and Vaniman, D.T., 1983, Tectonic implications of mid-Teritary dikes in west-central New Mexico: Geology, v. 11, p. 45-48.

Lipman, P.W., 1983, Cenozoic magmatism associated with extensional tectonics in the Rocky Mountains [abs.]: Geological Society of America Abstracts with Programs, v. 15, no. 5, p. 288.

Lovejoy, E.M.P., and Seager, W.R., 1978, Discussion of structural geology of Franklin Mountains, in Hawley, J.W., compiler, Guidebook to Rio Grande Rift in New Mexico and Colorado: New Mexico Bureau of Mines and Mineral Resources Circular 163, p. 68-69.

Lozinsky, R.P., 1986, Geology and late Cenozoic history of the Elephant Butte area, Sierra County, New Mexico: New Mexico Bureau of Mines and Mineral Resources Circular 187, 40 p., 2 plates, 1:25,000 scale.

Machette, M.N., 1978, Geologic map of the San Acacia quadrangle, Socorro County, New Mexico: U.S. Geological Survey Quadrangle Map GQ-1415, scale 1:24,000.

_____1985, Calcic soils of the southwestern United States, in Weide, D.L., ed., Soil and Quaternary geology of the southwestern United States: Geological Society of America Special Paper 203, p. 1-21.

_____1986, History of Quaternary offset and paleoseismicity along the La Jencia fault, central Rio Grande rift, New Mexico: Bulletin of the Seismological Society of America, v. 76, no. 1, p. 259-272.

_____1987, Neotectonics of the Rio Grande rift, New Mexico: Geological Society of America Abstracts with Programs, v. 19, no. 7 (in press).

Machette, M.N., and Colman, S.M., 1983, Age and distribution of Quaternary faults in the Rio Grande rift--Evidence from morphometric analysis of fault scarps [abs.]: Geological Society of America Abstracts with Programs, v. 15, no. 5, p. 320.

Machette, M.N., and McGimsey, R.G., 1983, Map of Quaternary and Pliocene faults in the Socorro and western part of the Fort Sumner 1° x 2° quadrangles, central New Mexico: U.S. Geological Survey Miscellaneous Field Studies Map MF-1465-A, scale 1:250,000.

Machette, M.N., and Personius, S.F., 1984, Map showing Quaternary and Pliocene faults in the east part of the Aztec 1° x 2° quadrangle and west part of the Raton 1° x 2° quadrangle, northern New Mexico: U.S. Geological Survey Miscellaneous Field Studies Map MF-1465-B, scale 1:250,000.

Machette, M.N., Personius, S.F., and Nelson, A.R., 1986, Late Quaternary segmentation and slip-rate history of the Wasatch fault zone, Utah [abs.]: EOS (Transactions of the American Geophysical Union), v. 67, no. 44, p. 1107.

Machette, M.N., Personius, S.F., Menges, C.M., and Pearthree, P.A., 1986, Map showing Quaternary and Pliocene faults in the Silver City 1° x 2° quadrangle and the Douglas 1° x 2° quadrangle, southeastern Arizona and southwestern New Mexico: U.S. Geological Survey Miscellaneous Field Studies Map MF-1465-C, scale 1:250,000.

Muehlberger, W.R., 1979, The Embudo fault between Pilar and Arroyo Hondo, New Mexico--an active intracontinental transform fault, in Ingersoll, R.A., ed., Guidebook to Santa Fe Country: New Mexico Geological Society, 30th Field Conference, p. 77-82.

Nakata, J.K., Wentworth, C.M., and Machette, M.N., 1982, Quaternary fault map of the Basin and Range and Rio Grande rift provinces, Western United States: U.S. Geological Survey Open-File Report 82-579, scale 1:2,500,000.

Nash, D.B., 1981, FAULT--A Fortran program for modelling the degradation of active normal fault scarps: Computers and Geosciences, v. 7, p. 249-266.

Otte, Carel, Jr., 1959, Late Pennsylvanian and Early Permian stratigraphy of the northern Sacramento Mountains, Otero County, New Mexico: New Mexico Bureau of Mines and Mineral Resources Bulletin 50, 111 p.

Pierce, K.L., and Colman, S.M., 1986, Effect of height and orientation (microclimate) on geomorphic degradation rates and processes, late-glacial terrace scarps in central Idaho: Geological Society of America Bulletin, v. 97, p. 869-885.

Pray, L.G., 1961, Geology of the Sacramento Mountains Escarpment, Otero County, New Mexico: New Mexico State Bureau of Mines and Mineral Resources Bulletin 35, 144 p.

Ramberg, J.B., Cook, F.A., and Smithson, S.B., 1978, Structure of the Rio Grande rift in southern New Mexico and west Texas based on gravity interpretation: Geological Society of America Bulletin v. 89, no. 1, p. 107-123.

Reiche, Parry, 1938, Recent fault scarps, Organ Mountains district, New Mexico: American Journal of Science, Series 5, v. 36, no. 216, p. 440-444.

Richardson, G.B., 1909, Description of the El Paso quadrangle, Texas: U.S. Geological Survey Geologic Atlas, Folio 116, 11 p.

Riecker, R.E., 1979, ed., Rio Grande Rift: Tectonics and Magmatism: Washington, D.C., American Geophysical Union, 438 p.

Sayre, A.N., and Livingston, Penn, 1945, Ground-water resources of the El Paso area, Texas: U.S. Geological Survey Water-Supply Paper 919, 190 p.

Scott, W.R., McCoy, W.D., Shroba, R.R., and Rubin, Meyer, 1983, Reinterpretation of exposed record of the two last cycles of Lake Bonneville, western United States: Quaternary Research, v. 20, no. 3, p. 261-287.

Seager, W.R., 1980, Quaternary fault system in the Tularosa and Hueco Basins, southern New Mexico and west Texas, in Dickerson, P.W., and Hoffer, J.M., eds., Trans-Pecos region, southeastern New Mexico and west Texas: New Mexico Geological Society 31st Annual Field Conference Guidebook, p. 131-136.

_____1981, Geology of the Organ Mountains and southern San Andres Mountains, New Mexico: New Mexico Bureau of Mines and Mineral Resources Memoir 36, 97 p., 4 plates, scale 1:31,250

Seager, W.R., and Morgan, Paul, 1979, Rio Grande rift in southern New Mexico, west Texas, and northern Chihuahua, in Riecker, R.E., ed., Rio Grande rift--tectonics and magmatism: Washington D.C., American Geophysical Union, p. 87-106.

Seager, W.R., Clemons, R.E., and Callender, J.F., eds., 1975, Guidebook of the Las Cruces country: New Mexico Geological Society Twenty-sixth Annual Field Conference Guidebook, 376 p.

Seager, W.R., Hawley, J.W., Kottlowski, F.E., and Kelley, S.A., 1987, Geology of east half of Las Cruces and northeast El Paso 1° x 2° sheets: New Mexico Bureau of Mines and Mineral Resources Geologic Map 57, 3 plates, scale 1:125,000.

Seager, W.R., Shafiqullah, M., Hawley, J.W., and Marvin, R.F., 1984, New K-Ar dates from basalts and the evolution of the southern Rio Grande rift: Geological Society of America Bulletin, v. 95, no. 1, p. 87-99.

Strain, W.S., 1966, Blancan mammalian fauna and Pleistocene formations, Hudspeth County, Texas: University of Texas at Austin, Texas Memorial Museum Bulletin 10, 55p.

Wallace, R.E., 1977, Profiles and ages of young fault scarps, north-central Nevada: Geological Society of America Bulletin, v. 88, no. 9, p. 1267-1281.

Weir, J.W., Jr., 1965, Geology and availability of Ground water in the northern part of the White Sands Missile Range and Vicinity, New Mexico: U.S. Geological Survey Water Supply Paper 1801, 78 p.

Wilson, C.A., and Myers, R.G., 1981, Ground water resources of the Solodad Canyon re-entrant and adjacent areas, White Sands Missile Range and Fort Bliss military reservation, Dona Ana County, New Mexico: U.S. Geological Survey Water Resources Investigations 81-645, 22 p.

Woodward, L.A., Callender, J.F., Seager, W.R., Chapin, C.E., Gries, J.C., shaffer, W.L., and Zilinski, R.E., 1978, Tectonic map of the Rio Grande rift region in New Mexico, Chihuahua, and Texas, in Hawley, J.W. compiler, Guidebook to Rio Grande rift in New Mexico and Colorado: New Mexico Bureau of Mines and Mineral Resources Circular 163, scale 1:1,000,000.

Zoback, M.L., and Zoback, Mark, 1980, State of stress in the conterminous United States: Journal of Geophysical Research, v. 85, no. B11, p. 6113-6156.

Zoback, M.L., Anderson, R.E., and Thompson, G.A., 1981, Cainozoic evolution of the state of stress and style of tectonism of the Basin and Range province of the western United States: Philosophical Transactions of the Royal Society of London, series A, v. 300, p. 407-434.

APPENDIX

Table 1.--Morphometric data for scarps on major Quaternary faults near White Sands Missile Range, New Mexico

[Symbols for the following tables: *, data not used in regression equations; ---, value not determined; Do., ditto; n, number of data pairs; r^2, coeffic ient of determination. Abbreviations: I.R., Isaacks Ranch alluvium; Pic., Picacho alluvium, Tor., Tortugas alluvium. Number of fault (shown in paren thesis) corresponds with those shown on fig. 1 and table 2).]

SAN ANDRES FAULT (3)
CENTRAL SEGMENT, LATEST PLEISTOCENE
SOUTHERN SEGMENT, EARLY HOLOCENE OR LATEST PLEISTOCENE

Profile number	Scarp angle (in degrees)	Scarp height (in m) Single (Hs)	Multiple (Hm)	Total (Ht)	Remarks
CENTRAL SEGMENT:					
m18-12	18.4	---	15.3	26.5	Tor.
m18-14	12.75	5.4	---	---	Pic.?
m18-15	7.5	3.4	---	---	I.R.?
m18-16	6.0	2.7	---	---	Do.
m18-17	14.75	---	6.9	13.0	Pic.?
m18-18	12.85	---	6.3	8.1	Pic.
m18-19	17.5	---	12.3	28.7	Tor.
m18-20	9.0	4.6	---	---	Tor.?
Regression equations:	θ =-3.1 + 20.3(log Hs)		n = 4	r^2 = 0.88	(n too small)
	θ = 3.0 + 13.1(log Hm)		n = 4	r^2 = 0.95	(n too small)
	θ = 4.2 + 9.5(log Ht)		n = 4	r^2 = 0.94	(n too small)
SOUTHERN SEGMENT:					
m18-1	23.75	---	---	14.0	
m18-2	23.75	---	5.5	11.6	
m18-3				8.7*	Double scarp.
m18-3a	13.75	2.8	---	---	Lower scarp.
m18-3a	18.25	3.6	5.9	---	Upper scarp.
m18-4	25.0	---	10.6	16.8	
m18-5	25.75	---	11.2	15.4	
m18-6	13.8	---	3.65	---	
m18-7	17.5	3.7	7.5	---	Pic.
m18-8	21.5	---	---	21.9	Tor.
m18-9	25.0	---	6.5	15.0	Pic.?
m18-10	17.75	4.1	6.5	---	Do.
m18-11	20.6	---	6.9	12.0	Pic.
m18-13	19.5	4.8	8.6	---	Do., overlaps central segment.
Regression equations:	θ = 4.0 + 23.3(log Hs)		n = 5	r^2 = 0.86	(n too small)
	θ = 5.0 + 18.6(log Hm)		n = 10	r^2 = 0.43	
	θ = 23.2 + 0.4(log Ht)		n = 7	r^2 = 0.00	(no significance)

* Data (total height of double scarp) not used in analysis.

Table 1.--Continued

ORGAN MOUNTAINS FAULT (4) NEAR COX RANCH
MIDDLE TO LATE HOLOCENE

Profile number	Scarp angle (in degrees)	Scarp height (in m) Single (Hs)	Multiple (Hm)	Total (Ht)	Remarks
m2-1	13.5	1.85	---	---	Or., youngest phase.
m2-2	15.3	---	2.85	---	Or., second youngest phase.
m2-3				6.25*	Double scarp.
m2-3a	15.5	---	2.75	---	Or.,older phase; upper scarp.
m2-3b	19.0	---	3.5	---	Or., older phase; lower scarp.
m2-4		---		5.2*	Double scarp.
m2-4a	12.0	1.6	---	---	Or., older phase; upper scarp.
m2-4b	19.5	---	4.6	---	Or., older phase; lower scarp.
m2-5	20.5	---	4.1	---	Or., older phase.
m2-6	21.5	---	4.5	---	Or., older phase.
m2-7	25.0	---	---	9.5	I.R., Ht minimum..
m2-8	23.5	---	5.8	---	Or., older phase.
m2-9	13.75	2.0	---	---	Or., young phase.
m2-10	26.5	---	---	>26.1	Tor.?, Ht minimum.
m2-11	26.25	---	9.9	15.5	Pic.?, Ht minimum.
Regression equations:	$\theta = 7.4 + 9.9(\log Hm)$		$n = 8$	$r^2 = 0.91$	

* Data for total height of double scarps not used in analysis

Table 1.--Continued

EAST FRANKLIN MOUNTAINS FAULT (6)
LATEST PLEISTOCENE OR EARLY HOLOCENE

[Additional abbreviations: G.H., Gold Hill alluvium; K.P., Kern Place alluvium; J.I, Jornada I alluvium; C.R., Camp Rice Formation, constructional surface.]

Profile number	Scarp angle (in degrees)	Scarp height (in m) Single (Hs)	Multiple (Hm)	Total (Ht)	Remarks
m17-1	24.25	---	5.8	9.3	G.H., Ht minimum.
m17-2	25.50	---	---	12.4	K.P., Ht minimum.
m17-3	15.50	3.5*	---	---	Old scarp on K.P., splay of main fault.
m17-4	21.50	3.7	---	---	I.R., young scarp.
m17-5	23.25	---	8.0	59.6	C.R., Ht minimum.
m17-6	18.75	---	4.6	8.9	G.H., Ht minimum.
m17-7	23.0	---	6.5	12.5	K.P.?, Ht minimum.
m17-8		---	---	10.9*	Double scarp.
m17-8a	14.0	2.7	4.0	---	K.P., lower scarp.
m17-8b	19.0	---	4.4	6.9	K.P., upper scarp.
m17-9	10.0	2.2*	---	---	K.P., old basin-splay.
m17-10	9.75	2.4*	---	---	Do.
m17-11	15.0	---	4.3	---	G.H.?
m17-12	18.6	---	4.6	---	G.H.?, S. of highway.
m17-13	22.0	3.2*	---	---	G.H., N. of highway.
m17-14	21.25	---	4.9	7.8	K.P., Ht, minimum.
m17-15	19.75	---	5.8	---	Do.
m17-16	19.5	---	12.0	34.8	J.I, Ht minimum.
m17-17	22.25	---	4.9	---	G.H.?
m17-18	21.5	---	6.6	30.3	J.I, Ht minimum.
m17-19	18.75	3.3	7.7	---	K.P.?, Ht minimum.
Regression equation:	$\theta = 12.9 + 9.3(\log Hm)$		$n = 14$	$r^2 = 0.10$	
	$\theta = 20.7 + 0.9(\log Ht)$		$n = 9$	$r^2 = 0.00$	(no significance)

* Data not used in analysis (Hs not on main fault, possibly older strand; Ht from double scarp).

Table 1.--Continued

ALAMOGORDO FAULT (7)
LATEST PLEISTOCENE OR EARLY HOLOCENE

Profile. number	Scarp angle (in degrees)	Scarp height (in m) Single (Hs)	Multiple (Hm)	Total (Ht)	Remarks
m30-1	18.25	---	5.5	7.1	East of Alamogordo.
m30-2	13.2	2.0	---	---	Do.
m30-3	20.4	---	5.6	---	Do.
m30-4	23.0	---	5.3	7.9	Do.
m30-5	17.0	2.9	4.3	---	Do.
m30-6	22.25	---	5.2	9.6	Do.
m30-7	21.0	---	7.0	---	Do.
m30-8	15.75	---	4.6	---	Do.
m31-1	27.25	---	9.8	---	South of Alamogordo.
m31-2	22.1	---	10.2	---	Do.
m31-3	25.25	---	10.5	---	Do.
m31-4	14.25	---	3.15	---	Do.
m31-5	21.75	---	4.9	6.1	Do.
Regression equation:	$\theta = 6.2 + 18.6(\log Hm)$		$n = 12$	$r^2 = 0.55$	
	$\theta = 29.1 - 10.6(\log Ht)$		$n = 4$	$r^2 = 0.00$	(n too small)

Table 2. Location, recency of movement, and size of some major faults near White Sands Missile Range, New Mexico

[Ages: h, Holocene(10 ka); vlp, latest Pleistocene (10-35 ka), lp, late Pleistocene (10-130 ka); mp, middle Pleistocene (130-750 ka); ep, early Pleistocene (750 ka-1.65 Ma) to Pliocene (1.65-5.0 Ma). Symbol e indicates scarp height estimated from topographic map. Types of fault movement, as determined from scarp morphology, age dating of faulted deposits, and (or) map pattern: segmented (segm) or recurrent (recur); n.d., not determined.]

No. on fig. 1, table 1	Fault name(s)	Location	Age of most recent movement	Measured scarp heights (m)	Age of displaced deposits	Fault length (km)	Type of fault movement	References
3	San Andres Mnts:	East front of San Andres Mountains:				106	Normal, recur., range-bounding.	Kelly, 1955; Kottlowski, 1955. Seager and others, 1987.
	Northern segment.	North of Rhodes Canyon.	lp?	n.d.	mp-lp	22	Do.	
	Central segment.	Rhodes Canyon south to Lead Camp Canyon.	vlp	3-29	mp-lp	48	Do.	
	South segment.	Lead Camp Canyon south to N.M. Highway 70.	vlp-h?	3-22	mp-vlp	36	Do.	Seager and others, 1987.
4	Organ Mountains	East front of Organ Mountains.	h (2)	2-26	mp-h	42	Normal, recur.; range-bounding.	Reiche, 1938; Seager, 1981; Seager and others, 1987; Gile, 1986, 1987.
5	Artillery Range	Basinward splay of Organ. Mtns fault.	vlp?				Normal, recur.; basin splay.	Seager, 1981; Seager and others, 1987.
6	East Franklin Mts.	East front of Franklin Mountains from Anthony Gap south to El Paso, Texas.	vlp-h	3-60	mp-vlp	45	Normal, recur., range-bounding.	Richardson, 1909; Sayre and Livingston, 1945; Harbour, 1968 Lovejoy and Seager, 1978; Seager, 1980.
7	Alamogordo:	West front of Sacramento Mountains:				57	Normal, recur., range-bounding.	Otte, 1959; Pray, 1961; Weir, 1965.
	North part.	East of Alamogordo	vlp-h?	2-10	lp-vlp			
	South part.	Southeast of Alamogordo	vlp-h?	3-11	lp-vlp			
	Intrabasin	Hueco Bolson, between El Paso and WSMR.	≤mp	<20	mp-lp?	10-35	Normal, recur., intrabasin.	Seager, 1980; Seager and others, 1987.